Journal of Power Sources

The effect of the pretreatment processes on the corrosion and stability of titanium porous transport layer in proton exchange membrane water electrolyzer

--Manuscript Draft--

Manuscript Number:	POWER-D-23-03144
Article Type:	Research Paper
Section/Category:	Polymer Electrolyte Membrane Fuel Cells: SCITECH
Keywords:	proton exchange membrane water electrolyzer (PEMWE), porous transport layer (PTL), titanium felt, pretreatment, corrosion
Corresponding Author:	Mingruo Hu, PH.D. Shanghai, CHINA
First Author:	Zheng Zhou
Order of Authors:	Zheng Zhou
	Kequan Ye
	Qing Wang
	Mingruo Hu, PH.D.
	Xiaoyu Hu
	Sibo Wang
	Chengyu Hu
	Guangyi Cao
Manuscript Region of Origin:	CHINA
Abstract:	This article investigates the impact of pretreatment processes on pristine titanium (Ti) porous transport layers (PTLs) used in proton exchange membrane water electrolyzers (PEMWEs). Ultrasonic cleaning and acid etching are commonly employed pretreatment methods, yet their precise effects on PTL surface states and electrolyzer performance remain unclear. Ten anode PTLs are crafted using varying pretreatment processes, combining electrochemical testing of single electrolyzers with physical characterizations of the PTLs to disclose these mechanisms. Acid etching aims to remove the Ti oxide film atop pristine Ti felt, addressing potential dislocations and cracks from manufacturing while forming a protective titanium hydride (TiHx) film. Notably, dislocations and cracks are identified as culprits inducing side reactions, such as Ti corrosion during electrolyzer operation, leading to the appearance of high frequency (HF) arcs in electrochemical impedance spectroscopy (EIS) curves and degrading electrolyzer performance. Contrastingly, ultrasonic cleaning is found to exacerbate dislocation and crack formation, worsening the surface condition of Ti PTL during both pretreatment and subsequent electrolyzer operation. Ultimately, this study highlights that coating a Ti PTL with an imperfect surface condition offers only temporary protection. Thus, achieving an optimal Ti PTL surface condition through suitable pretreatment processes is essential for enhancing electrolyzer performance.
Suggested Reviewers:	Hongtan Liu, Phd Professor, University of Miami hliu@miami.edu
	Quentin Meyer, Phd Fuel Cell Cluster Leader and Lab Manager, University of New South Wales q.meyer@unsw.edu.au
	Fengjing Jiang, Phd Senior engineer, Basque Research and Technology Alliance jiangfengjing@googlemail.com
	Hang Guo, Phd

	Professor, Beijing University of Technology hangguo@sohu.com
	Awotwe Tabbi Wilberforce, Phd Assistant Professor, King's College London tabbi.wilberforce@kcl.ac.uk
	Xi Li, Phd Professor, Huazhong University of Science and Technology lixi_wh@126.com

Dear editors

We submit our manuscript “The effect of the pretreatment processes on the corrosion and stability of titanium porous transport layer in proton exchange membrane water electrolyzer” to Journal of Power Sources. The important content of this article is concluded as follows,

This article investigates the impact of pretreatment processes on pristine titanium (Ti) porous transport layers (PTLs) used in proton exchange membrane water electrolyzers (PEMWEs). Ultrasonic cleaning and acid etching are commonly employed pretreatment methods, yet their precise effects on PTL surface states and electrolyzer performance remain unclear. Ten anode PTLs are crafted using varying pretreatment processes, combining electrochemical testing of single electrolyzers with physical characterizations of the PTLs to disclose these mechanisms. Acid etching aims to remove the Ti oxide film atop pristine Ti felt, addressing potential dislocations and cracks from manufacturing while forming a protective titanium hydride (TiHx) film. Notably, dislocations and cracks are identified as culprits inducing side reactions, such as Ti corrosion during electrolyzer operation, leading to the appearance of high frequency (HF) arcs in electrochemical impedance spectroscopy (EIS) curves and degrading electrolyzer performance. Contrastingly, ultrasonic cleaning is found to exacerbate dislocation and crack formation, worsening the surface condition of Ti PTL during both pretreatment and subsequent electrolyzer operation. Ultimately, this study highlights that coating a Ti PTL with an imperfect surface condition offers only temporary protection. Thus, achieving an optimal Ti PTL surface condition through suitable pretreatment processes is essential for enhancing electrolyzer performance.

Finally, we state that we have complied with Elsevier's ethical requirements. We declare the manuscript has not been published before nor submitted to another journal for the consideration of publication.

Thank you very much for your attention and consideration.

Sincerely yours,

Mingruo Hu

Highlights

- Dislocations and cracks in the PTL induce the corrosion of Ti metal during electrolyzer operation.
- The high frequency arc of the EIS curve represents the happening of Ti corrosion.
- The ultrasonic cleaning process exacerbates dislocations and cracks on the surface of a Ti PTL.
- A suitable acid etching process forms a good surface condition with TiH_x protecting film on a PTL.
- Acquiring a good surface condition of Ti felt is the priority task before conducting coating.

The effect of the pretreatment processes on the corrosion and stability of titanium porous transport layer in proton exchange membrane water electrolyzer

Zheng Zhou [a], Kequan Ye [a], Qing Wang [a], Mingruo Hu [a*], Xiaoyu Hu [a], Sibo Wang [a], Chengyu Hu [a,b], Guangyi Cao [a]

[a] G-Lab, Institute of Fuel Cell, Shanghai Jiao Tong University, 800 Dongchuan Rd, 200240, China

[b] Hugh McRoberts Secondary, 8980 Williams Rd, Richmond, BC V7A 1G6, Canada

Abstract

This article investigates the impact of pretreatment processes on pristine titanium (Ti) porous transport layers (PTLs) used in proton exchange membrane water electrolyzers (PEMWEs). Ultrasonic cleaning and acid etching are commonly employed pretreatment methods, yet their precise effects on PTL surface states and electrolyzer performance remain unclear. Ten anode PTLs are crafted using varying pretreatment processes, combining electrochemical testing of single electrolyzers with physical characterizations of the PTLs to disclose these mechanisms. Acid etching aims to remove the Ti oxide film atop pristine Ti felt, addressing potential dislocations and cracks from manufacturing while forming a protective titanium hydride (TiHx) film. Notably, dislocations and cracks are identified as culprits inducing side reactions, such as Ti corrosion during electrolyzer operation, leading to the appearance of high frequency (HF) arcs in electrochemical impedance spectroscopy (EIS) curves and degrading electrolyzer performance. Contrastingly, ultrasonic cleaning is found to exacerbate dislocation and crack formation, worsening the surface condition of Ti PTL during both pretreatment and subsequent electrolyzer operation. Ultimately, this study highlights that coating a Ti PTL with an imperfect surface condition offers only temporary protection. Thus, achieving an optimal Ti PTL surface condition through suitable pretreatment processes is essential for enhancing electrolyzer performance.

* Corresponding author.
E-mail address: mingruohu@sjtu.edu.cn

Key Words: proton exchange membrane water electrolyzer (PEMWE), porous transport layer (PTL), titanium felt, pretreatment, corrosion

1 Introduction

The burgeoning worldwide necessity for energy consumption and the imperative of curbing carbon emissions have emerged as the primary catalysts fueling the pursuit of renewable energy sources. The exponential advancement of renewable energy technology in recent decades has engendered a prospective ecological future for energy production, however, has also led to the challenge of intermittent power generation on the grid [1]. To mitigate this oscillation, the development of large-scale hydrogen production through water electrolysis from renewable energy sources has emerged as a potential solution [2–4]. Among the prevailing types of water electrolyzer, namely, alkaline water electrolyzer (AWE), proton exchange membrane water electrolyzer (PEMWE), and solid oxide water electrolyzer (SOWE), PEMWE stands out due to its faster response, more compact structure, and higher operating current density. Nonetheless, the employment of precious metals as catalysts and coatings in PEMWE has resulted in concerns regarding its cost-effectiveness, thus, its installed capacity remains lower than that of AWE [5]. The main components of PEMWE stacks comprise the catalyst coated membrane (CCM), porous transport layer (PTL), and bipolar plate (BPP). PTL accounts for around 17% of the total stack cost [6], playing an essential role in mass and electron transfer. Unlike fuel cells, electrolyzers entail higher anode voltage (~2V) [5], hence, carbon paper, which is susceptible to corrosion at high potential, cannot be employed as a stable PTL at the anode for a long time. Therefore, this is the first reason that Ti-based materials, including Ti mesh [7–9], sintered Ti powder [10,11], sintered Ti felt [12,13], and thin/well-tunable liquid/gas diffusion layers (TT-LGDL) made from Ti foils by masking and wet-etching[14,15], are the commonly used anode PTLs. The usage of Ti mesh as a PTL is constrained due to its small contact area with the catalyst layer, resulting in an inferior catalyst utilization rate, and high resistance of mass transfer [8,9]. TT-LGDL improves the electrochemical performance due to its optimal mass transfer channel and flat contact interface, however, its processing intricacy [14] has not garnered extensive use.

Uncoated Ti felt-based PTL is frequently utilized in short-term I-V performance testing after it

is first pretreated by ultrasonic cleaning to remove impurities or contaminants [16–20] and then by acid etching to thin the passivation (oxide) film (mainly including TiO_2) [20–22]. To clean the stains on the PTL surface, sequential ultrasonic treatment of acetone-isopropanol-deionized water is commonly used, with each step lasting for 15 minutes [20,21,23]. However, some studies have shown that ultrasound can cause changes to the surface of titanium materials [24,25], for example, ultrasound-induced structural damage in TiO_2 has been observed, including refinement, structural damage, and changes in the dense layer [24–26]. In addition, cavitation induced by ultrasound has been found to have a higher propensity to initiate Ti corrosion in the presence of halogen species, such as fluorine (F) [27,28]. Therefore, the application of a suitable ultrasonic cleaning process needs to be addressed to avoid change and damage to the surface of Ti PTLs during this pretreatment, however, it seems that currently there is a lack of related research based on the PEMWE performance. Moreover, acid etching is also considered a prerequisite step to form titanium hydride (TiH_x) before PTL coating [23]. The formation of titanium hydride can slow the process of oxidation before coating and increase the adhesion between the coating layer and the titanium surface [29,30], which is important for the long-term testing of a PEMWE. Hydrochloric acid or oxalic acid is usually used to etch the oxide film (mainly containing passivation layer, TiO_2) on the surface of titanium [21,23,31] to acquire a reasonable thickness of TiH_x [23,32], of which hydrochloric acid is chosen because it has a higher etching rate and can help to generate TiH_x to delay the further formation of surface passivation [23,32].

Moreover, considering that the acidity of a Nafion membrane is equivalent to 0.5 M sulfuric acid [33], this is the second reason that titanium is often chosen as the material of PTL to relieve the corrosion (i.e., material loss due to metal ions released from a metal body) due to that its stability in an acidic environment is better than other metals such as stainless steel [34]. This is because, even at room temperature, the passivation layer (TiO_2) is easy to form on the surface of the pure titanium metal; moreover, oxygen evolution reaction (OER) integrating the anode high potential can further oxide the Ti-based PTL [35], therefore, a thicker passivation layer (TiO_2) can be formed to protect Ti metal from the corrosive environment in the electrolyzer, however, in the meantime, resulting in a poor conductivity [36, 37] and an increase in the ohmic resistance, i.e., high frequency resistance (HFR) [38]. As a result, significant research has focused on PTL surface coating to prevent performance degradation caused by oxidation [20,33,34], in which comparisons with uncoated PTL

were also conducted: (1) Some research showed that the uncoated Ti PTLs could demonstrate comparable performance with coated PTLs in the initial stage of their lifetime, but, they would lose their stability with time [16,20,33] to decrease the PEMWE performance greatly; (2) Differently, other research found that the PEMWE with uncoated PTL performed poorly even in the initial stage of its lifetime when compared to that of a PEMWE with coated PTL [32,35], which was normally attributed to the higher HFR (Ohmic resistance); (3) However, results of Stiber et al. [34] indicated that the poor performance of the PEMWE with uncoated unstable PTL maybe was not due to HFR but the appearance of high frequency (HF) arc (which was considered as a kind of charge transfer resistance in [34]), because it disappeared after a coated PTL was adopted and the related performance of the PEMWE was increased; (4) Moreover, another research even found that the HF arc still appeared even if the coating was exerted on the Ti PTL [32].

Based on the above survey of the current research, it seems that there is a lack of understanding of the mechanisms how the ultrasonic cleaning process affects the surface condition of a Ti PTL and its performance during operation, and a lack of understanding of the mechanisms how TiH_x formed in the acid etching process helps improve the surface condition of a Ti PTL; moreover, there is also a lack of understanding of the mechanisms how the pretreatment processes of PTL affect the function of a coating compared to that of an uncoated PTL; and finally, there is a lack of understanding of the mechanisms of the appearance of the HF arc for electrolyzers with uncoated PTL or even coated PTL and its effect on the electrolyzer performance.

In this article, ten anode PTLs are fabricated based on different designs of pretreatment processes including acid etching and ultrasonic cleaning. By integrating the electrochemical testing (I-V test and EIS test) for single electrolyzers using these ten different PTLs with the physical characterizations (XRD, XPS, SEM, and EDS) for the PTLs, the above-mentioned lack of understanding of mechanisms and other possible mechanisms related to the PTLs are tried to be disclosed. For example, the purpose of acid etching is to eliminate the Ti oxide film on the top surface of a pristine Ti felt, in which dislocations and cracks may exist due to manufacturing, and to form a good TiH_x film for protection; it is the dislocations and cracks that are found to induce side reactions such as the Ti corrosion during the operation of an electrolyzer, which result in the appearance of the HF arc in the EIS curve and worsens the performance of the electrolyzer; ultrasonic cleaning is found to lead to the formation of more dislocations or cracks, i.e., worsening

the surface condition of Ti felt during the pretreatment process and the later operation in electrolyzers. Finally, it is found that coating exerted on a Ti felt with poor surface condition may only supply temporary protection, therefore, good surface condition of Ti felt should be first acquired based on suitable pretreatment processes before the coating is applied.

2 Experimental

2.1 Parameters of the single electrolyzer

The parameters of the single electrolyzer are listed in Table 1. Catalyst Coated Membrane (CCM) method was used [36] to coat the Ir ink and Pt/C ink onto both sides of a membrane. The sealing material is presented in Table 1 except that when 48-15-CP (as shown in Table 2) was used, and the thickness of PTFE on the anode side was adjusted to 0.4 mm to match the thickness of 48-15-CP. When no special explanation was presented, a new anode PTL, CCM, and a new cathode gas diffusion layer (GDL) were always used, and both the anode and cathode Ti flow field plates (which were not coated with precious metal) were always polished with 1500 grit sandpaper before assembling and testing a new electrolyzer to eliminate the possible effect of decay.

Table 1 Specification of the single electrolyzer

Items		Specification
Active area		4 cm^2
Material of the CCM	Ir loading of the anode side	1.28mg·cm^{-2} (JM 16000: Ir black)
	Pt loading of the cathode side	0.32mg·cm^{-2} (JM 4100: 40% Pt/C)
	Ionomer dispersion	5% (Dupont: D520)
	Membrane	183 um（Dupont: Nafion 117）
Material of Anode PTL	Pristine Ti felt	0.4 mm (Bekaert 2GDL10-0.4)
	Carbon paper (For 48-15-CP)	0.19 mm Carbon paper (Toray 060)
Material of Cathode GDL	Backing layer	0.19 mm Carbon paper (Toray 060)
	Carbon black in the Microporous layer (MPL)	XC-72 (Vulcan)
Sealing	Polytetrafluoroethylene (PTFE)	0.3 mm for anode 0.15 mm for cathode
Flow field plate	Serpentine	2 channels
Assembling	Screw number	6
	Torque	1.5 N·m

2.2 Fabrication of PTLs based on different pretreatment of pristine Ti felt

In this research, all the Ti felts after pretreatment were recorded as Ti PTL, and Table 2 lists 10 different PTLs and their related pretreatment processes. Moreover, before the pretreatment, all the pristine Ti felt was stored in a vacuum tank to ensure as much consistency as possible in their initial state. The two general processes of pretreatment are as follows:

(1) The ultrasonic cleaning pretreatment

Acetone, isopropyl alcohol, and deionized water were used as cleaning agents during the ultrasonic cleaning. Table 2 lists the total time for an ultrasonic cleaning process, and the

duration of the ultrasonic cleaning in each agent remained equal, e.g., for the PTL named 12-15 as shown in Table 2, Ti felt was ultrasonically cleaned in acetone, isopropanol, and deionized water for 4 minutes each.

(2) The acid etching pretreatment

Ti felt was etched in a water bath with 36 wt% hydrochloric acid at 52℃ to thin the passivation layer on its surface; after that, the Ti felt was ultrasonically cleaned in deionized water for 3 minutes to remove residual hydrochloric acid.

Moreover, as shown in Table 2, the 48-15-CP represents a two-layer PTL, i.e., a pretreated Ti felt was overlaid by a Toray 060 carbon paper, of which the carbon paper contacted directly with the anode catalyst layer in the single electrolyzer. The PTL named 48-15-Pt represents that a pretreated Ti felt was further coated with a 10 nm thickness Pt (platinum) film which contacted directly with the anode catalyst layer in the single electrolyzer. The Pt coating lasted for 15 seconds by utilizing a high vacuum coating machine (Q 150T ES plus, Quorum).

Table 2 Characteristics of 10 different Ti PTLs

No.	PTL Name	Ultrasonic cleaning Time (min)	Acid etching time (min)	Note for pretreatment and structure
1	Pristine	0	0	Pristine Ti felt directly used as the anode PTL
2	0-5	0	5	Only acid etching for 5 min
3	0-10	0	10	Only acid etching for 10 min
4	0-15	0	15	Only acid etching for 15 min
5	12-15	12	15	First, ultrasonic cleaning for 12 min; Then, acid etching for 15 min
6	24-15	24	15	First, ultrasonic cleaning for 24 min; Then, acid etching for 15 min
7	48-15	48	15	First, ultrasonic cleaning for 48 min; Then, acid etching for 15 min
8	EA-48-15	48	15	First, exposing to the environment atmosphere for one week; Then, ultrasonic cleaning for 48 min; In the end, acid etching for 15 min
9	48-15-CP	48	15	First, ultrasonic cleaning for 48 min; Then, acid etching for 15 min; After that, overlaying carbon paper (Toray 060) on the pretreated Ti felt to form the two-layer PTL
10	48-15-Pt	48	15	First, ultrasonic cleaning for 48 min; Then, acid etching for 15 min; After that, coating Pt onto the pretreated Ti felt for 15s

2.3 Testing and Characterization

2.3.1 Single electrolyzer testing

The I-V curve was tested based on a constant current mode set on the Land CT2001B DC power source. The testing current increased from 0A to 8A (i.e., 2A·cm^{-2}) including thirty sampling points, each of which lasted 30 seconds. In addition, after an I-V curve was acquired, the EIS testing was conducted on Gamry Reference 3000 Potentiostat/Galvanostat & 30 K Booster @ 0.4 A (0.1 A·cm^{-2}), and the AC amplitude was set at 10% of the DC voltage. During the testing, the single electrolyzer temperature was kept at 80℃ while the anode input deionized water was also heated to 80℃, and its flow rate was set at 2.7ml·min^{-1}.

Moreover, if there is no special explanation, the performance comparison between different single electrolyzers was always conducted between the first I-V testing circles after the electrolyzers were assembled. However, for the case of cycling testing, e.g., the Fig. 5 of this paper, multiple I-V testing circles were conducted for electrolyzer with EA-48-15 PTL, which are differentiated by the circle numbers, i.e., C20, C40,……, C100.

2.3.2 Material characterization

The cross-section of titanium fiber was obtained based on the three-ion beam cutter (EM TIC 3X, Leica). The microstructures of the samples were observed through scanning electron microscopy (SEM, JSM-7800F, JEOL) with an accelerating voltage of 5kV. Different titanium valences on the surface of the Ti PTLs were determined using X-ray Photoelectron Spectroscopy (XPS, K-Alpha, Thermo Scientific), and the data fitting process was accomplished based on Advantage software. X-ray diffraction (XRD, PANanalytical, Netherlands) was chosen to identify the possible composition of the Ti PTLs.

3 Results

3.1 Effect of acid etching

Although ultrasonic cleaning is normally the first step of the pretreatment process of a pristine Ti felt, it can arouse complicated physical phenomena discussed in Section 3.2, therefore, for the simplicity of research, only the acid etching process was studied in this Section, i.e., no ultrasonic cleaning was conducted before acid etching.

Fig. 1(a) presents the effect of the acid etching time of the Ti felt on the I-V performance of the single electrolyzer. As shown in Fig. 1(a), the performance is improved dramatically when the etching time increases from 0 min (i.e., no acid etching, the pristine Ti felt was used as the anode PTL) to 15 min. It can be explained based on the EIS curves shown in Fig. 1(b), which was tested @ 0.1 $A \cdot cm^{-2}$. As shown in Fig. 1(b), two characteristics can be found, i.e.,

(1) When the acid etching time increases, the ohmic resistance (HFR) seems hardly changed, i.e., there is no significant difference in the HFR before and after the etching, which suggests that the surface Ti oxide film (mainly including the passivation layer, i.e., TiO_2 due to its highest peak shown in Fig. 3) on a pristine felt is pretty thin, leading to a minor effect on the electron transfer (i.e., a minor effect on the ohmic resistance) through this film. Consequently, the electron transfer ability in the thin passivation layer of the PTL does not contribute significantly to the performance of the electrolyzer. This means the improvement of the I-V performance shown in Fig. 1 (a) was not derived from the reduction of the ohmic resistance, which was considered by other studies [23,32] as an important reason for the improvement of the performance due to thinning of the passivation layer (i.e., TiO_2 layer).

(2) High-frequency (HF) arcs (the left arc on the EIS curve) are found in Fig. 1(b) for the cases of 0-0 PTL (i.e., Pristine PTL), 0-5 PTL, and 0-10 PTL. They have the same frequency range from 300k Hz to 7.5k Hz. Moreover, it is easy to find that the diameter of the HF arc decreases dramatically when the etching time increases and it seems to disappear when the etching time is 15 minutes for the case of 0-15.

Based on the above findings, it is concluded that the decrease and disappearance of the HF arc with the increasing acid etching time is the dominant reason for the improvement of the I-V performance shown in Fig. 1(a).

Moreover, XRD testing and XPS testing were further conducted to elucidate the possible composition and the possible Ti valence state on the surface of the Ti felt for the case of 0-0 PTL (Pristine PTL) and the case of 0-15 PTL. As shown in Fig. 2, $TiH_{1.5}$ was detected by the XRD testing after the hydrochloric acid etching pretreatment was finished, which was also recorded by Bystron et al [23,32]. The formation of TiH_x (which can achieve a maximum ratio of H/Ti to 2[23]) is probably derived from the following process: during the etching period, the surface Ti oxide film (mainly including the passivation layer, i.e., TiO_2) is first removed by the concentrated hydrochloric acid solution, and then the inner Ti^0 (pure Ti metal) is exposed to react directly with hydrochloric acid to form TiH_x (Ti hydride) film [23,42] according to Equation (1) and Equation (2) on the top of the surface of a Ti fiber (e.g., in [37], x=2).

$$2Ti + 6H^+ \rightarrow 2Ti^{3+} + 6H \quad (1)$$

$$Ti + xH \rightarrow TiH_x \quad (2)$$

In addition, once the acid etching pretreatment is finished, the PTL is normally stored in the ambient air for further utilization, therefore, part of the TiH_x film on the top surface of a Ti fiber reacts with the oxygen in the air to be transformed again into different Ti oxides (i.e., a new Ti oxide film is formed again on the top of the TiH_x film) according to Equation (3), which is a process that gradually replaces H atoms in the lattice of TiH_x with O atoms to finally form TiO_2 [38,39].

$$TiH_x \rightarrow TiH_{x-y} \rightarrow TiO \rightarrow Ti_2O_3 \rightarrow Ti_3O_5 \rightarrow TiO_2 \quad (3)$$

As a result, as shown in Fig. 3, the XPS peaks of Ti^{2+}, Ti^{3+}, and Ti^{4+} of the 0-15 PTL still exist. Furthermore, some more information is also found in Fig. 3 when comparing the XPS peaks of different valences of Ti for the case of 0-15 PTL to those of 0-0 PTL (the Pristine PTL):

(1) The peak of Ti^0 (pure Ti metal) for the case of 0-15 PTL is higher than that of 0-0 PTL (the Pristine PTL), this is probably because the density [40] of the formed TiH_x film on the 0-15 PTL is smaller than that [41] of the Ti oxides film (mainly including TiO_2) on the pristine Ti felt (X-rays are more penetrating in less dense materials [42]), therefore, the X-ray signal can be easier to reach the inner Ti^0 (pure Ti metal) to form a higher Ti^0 peak for the case of 0-15 PTL than that for the case of 0-0 PTL (the Pristine PTL).

(2) Moreover, the XPS peak of Ti^{4+} for the case of 0-15 PTL is lower than that of 0-0 PTL (the Pristine PTL), this is probably because the transformed Ti^{4+} (TiO_2) is derived from the TiH_x according to Equation (3), although it appears on the very top surface of the Ti felt, it is the

last product of Equation (3). Therefore, its amount is small to result in a lower peak of Ti^{4+} for the case of 0-15 PTL than that of 0-0 PTL (the Pristine PTL).

(3) In addition, the XPS peaks of Ti^{2+} and Ti^{3+} for the case of 0-15 PTL are higher than that of 0-0 PTL (the Pristine PTL). This explains that there is newly formed Ti^{2+} and Ti^{3+} in the form of Ti oxides on the very top surface of the Ti felt according to Equation (3). Due to the smaller amount of Ti^{4+} explained in (2), it is easier for the X-ray signal to detect them to form a higher Ti^{2+} and Ti^{3+} peak (i.e., less attenuation of X-ray signal) for the case of 0-15 PTL than that for the case of 0-0 PTL (the Pristine PTL).

Furthermore, the formation of TiH_x in the concentrated acid solution demonstrates that Ti hydride is at least relatively chemically stable in an acid solution [23], therefore, the formed TiH_x film is expected to exert better corrosion protection for the PTL than the layer of TiO_2 on the surface of pristine PTL does during the OER reaction of the anode. In addition, the formation and coverage of TiH_x are expected to be improved with the increase in etching time, which could be correlated to the change in the size of the HF arc shown in Fig. 1(b), i.e., the size of HF arc decreases from the case when the Pristine PTL (i.e. no acid etching) was used to the case when 0-10 PTL was used and finally the HF arc disappears when the 0-15 PTL was used (i.e., the Ti felt experienced enough time of acid etching). Therefore, I-V performance was improved as presented in Fig. 1(a). Detailed mechanisms of how the formation and coverage of TiH_x are related to the change in the size of the HF arc will be discussed in Section 4 of this paper.

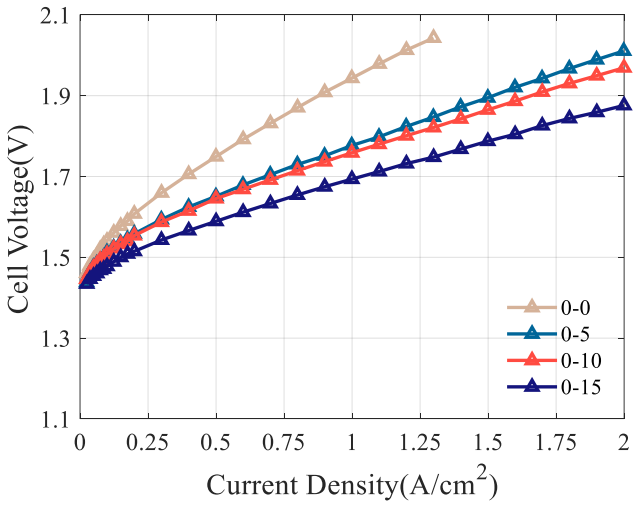

(a) Effect of acid etching time on the I-V curve.

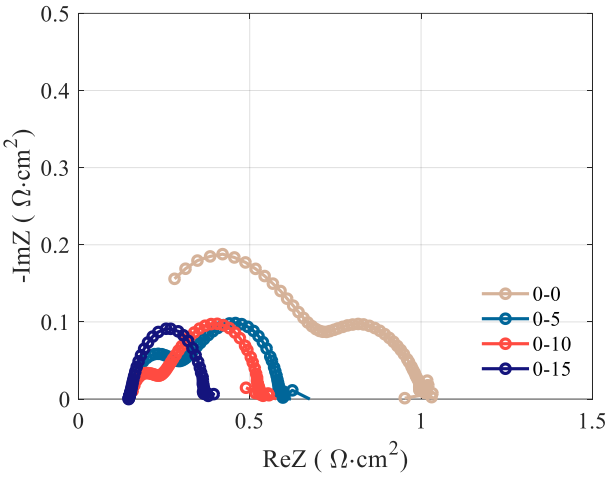

(b) Effect of acid etching time on the EIS curve @ 0.1 A·cm^{-2}.

Fig.1 Effects of acid etching time on the performance of the electrolyzer in the first circle.

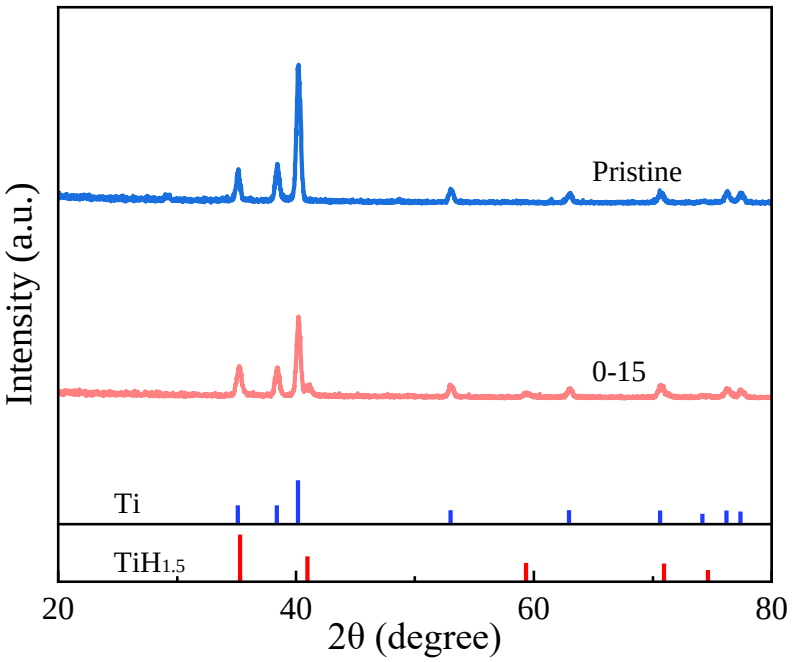

Fig. 2 XRD results for Pristine and 0-15 Ti PTL.

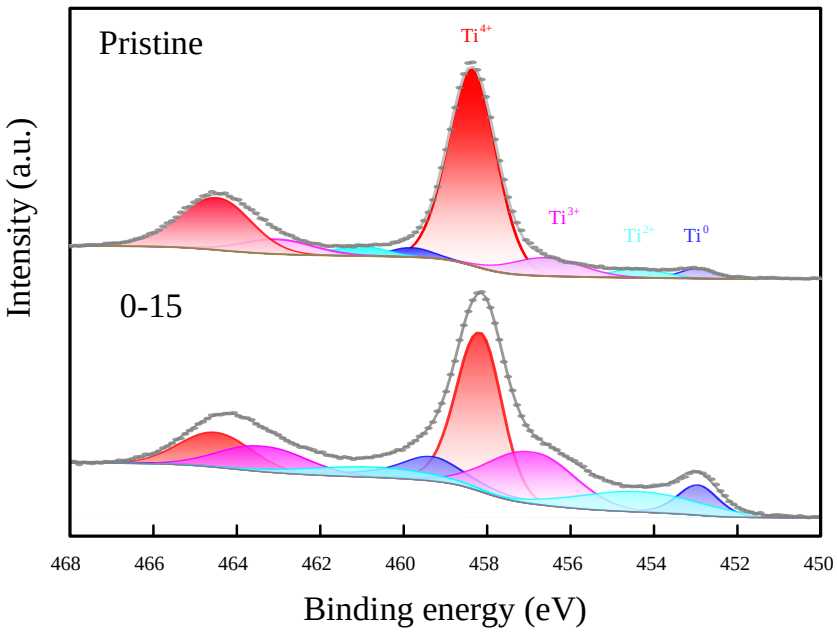

Fig. 3 Ti 2p XPS profiles and deconvolution results for the Pristine PTL (0-0 case) and 0-15 PTL.

3.2 Effect of ultrasonic cleaning

As mentioned in Section 1 of this paper, the ultrasonic cleaning process has been considered to help remove impurities or contaminants [20,23] on a pristine Ti felt, and it is normally conducted before the acid etching process. In this Section, different ultrasonic cleaning processes were tried to find the best performance for a single electrolyzer. Since the ultrasonic cleaning process is normally followed by the acid etching process, the optimal acid etching time, i.e., 15 minutes, concluded in Section 3.1, was set in this Section for the acid etching after the ultrasonic cleaning. For example, in this Section, the 12-15 PTL means the Ti felt was first ultrasonically cleaned for 12 minutes and then etched with acid for 15 minutes. Moreover, the optimal performance of Section 3.1, i.e., acquired from the electrolyzer with 0-15 PTL, is employed as the basis for discussion in this Section.

As shown in Fig. 4(a), the addition of the ultrasonic cleaning process before acid etching does not bring the expected performance improvement, i.e., three electrolyzers with the PTLs (12-15, 24-15, and 48-15) experiencing ultrasonic cleaning show poorer performance than that of the case with 0-15 PTL. More importantly, with the increasing ultrasonic cleaning time, the related I-V performance becomes worse, and the 48-15 PTL (i.e., the Ti felt experiencing the longest ultrasonic cleaning time) leads to the worst performance. The EIS curves shown in Fig. 4(b) and 4(c) match the I-V performance shown in Fig. 4(a), i.e., with the increasing ultrasonic cleaning time, the related

total EIS resistance becomes larger, and the 48-15 PTL leads to the largest total EIS resistance. More importantly, the HF arc appears again and it becomes much more prominent with the increasing ultrasonic cleaning time as shown in Fig. 4(b) and Fig. 4(c), i.e., the electrolyzer with the 48-15 PTL presents a much larger HF arc. The reason might be attributed to the damage of the Ti oxide film (mainly including the passivation layer, i.e., TiO_2) on the surface of the Ti felt due to the so-called cavitation derived from the ultrasonically produced excessive mechanical energy [24–26]. Therefore, a suitable surface condition might not be established, which would not lead to a good TiH_x film during the later acid etching process.

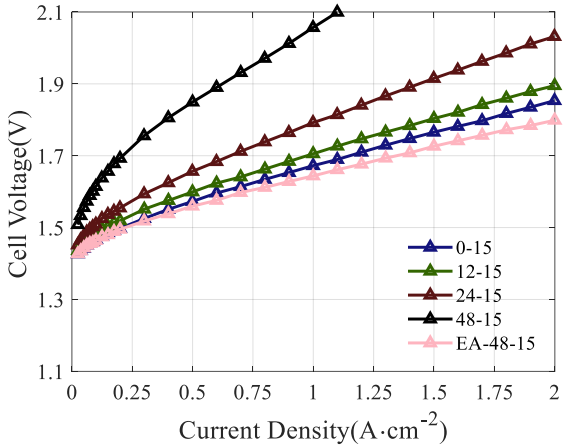

(a) Effect of ultrasonic time on the I-V curve with 15 min acid etching.

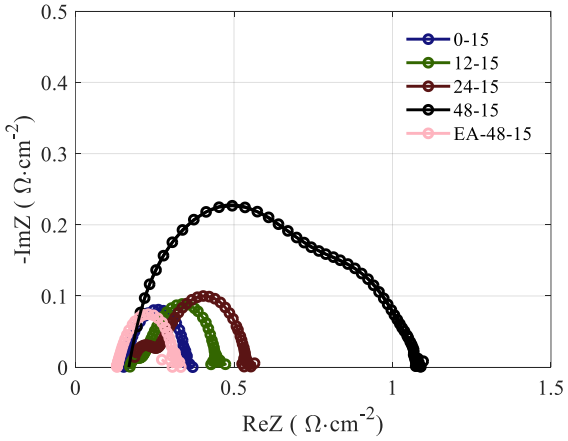

(b) Effect of ultrasonic time on the EIS curve (@0.1 A·cm^{-2}) with 15 min acid etching.

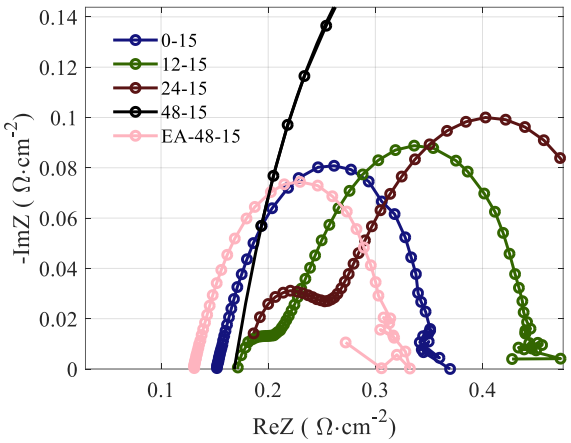

(c) Partially enlarged view of Figure (b) in high frequency domain.

Fig. 4 Effects of ultrasonic time on the performance of the electrolyzer in the first circle.

To initially prove this speculation, another new piece of Ti felt was exposed directly to the environment atmosphere (EA) at room temperature for one week, i.e., trying to form a much more protective Ti oxide film (mainly including the passivation layer, i.e., TiO_2) on the surface of Ti felt. After that, the Ti felt was further ultrasonically cleaned for 48 minutes and then etched in acid for 15 minutes. The resulting PTL is called EA-48-15 as presented in Table 2. As shown in Fig. 4(a), expected results are acquired: the performance of the single electrolyzer with EA-48-15 PTL, i.e., the I-V curve designated by EA-48-15 is much better than that with 48-15 PTL, for example, the voltage of EA-48-15 reaches 1.80 V at 2 $A \cdot cm^{-2}$, which is the lowest value compared to those of the other cases at the same current shown in Fig. 4(a). This probably means that the one-week pre-oxidation in the environment atmosphere formed much thicker and more protective Ti oxide film on the surface of Ti felt to resist the surface damage from cavitation during the ultrasonic cleaning process [43], and it thus led to a good TiH_x film formed during the acid etching process. To prove this conjecture, a total of 100 I-V testing circles were conducted for the electrolyzer with EA-48-15 PTL as shown in Fig. 5(a), and the related EIS curves were tested after every 20 I-V testing circles as shown in Fig. 5(c). Multiple I-V testing circles of Fig. 5 are differentiated by the circle numbers, i.e., C20, C40, C60, ……, C100 (refer to the definition of Section 2.3.1). As shown in Fig. 5(b), during the 100 I-V circles, the I-V performance gradually becomes poorer, for example, the voltage of the C100 is around 1.86 V vs. 1.80 V of the C1 @ 2$A \cdot cm^{-2}$, i.e., an increase of 60 mV. However, as shown in Fig. 5(c), it is easy to find: (1) The HF arc does not exist in all the testing circles, i.e., only one arc exists in each testing circle, which is considered as the kinetic (rate-limiting) resistance

[44] of the oxygen evolution reaction (OER), and its diameter hardly changes, i.e., the rate of the OER is kept the same; (2) The ohmic resistance is gradually increased. Based on the above two characteristics, it can be concluded that: (1) Exposing the Ti felt directly to the environment atmosphere at room temperature for one week did help to form a much thicker Ti oxide film (mainly including the passivation layer, i.e., TiO_2) on the surface of Ti felt, therefore, enough protection was supplied to eliminate the damage from the cavitation of the ultrasonic cleaning; as a result, the following acid etching process could form a good film of TiH_x to cover the whole surface of the Ti felt, leading to the disappearance of HF arc. (2) Considering that TiH_x has as good electron conductivity as Ti metal [45], the increased ohmic resistance with the increased I-V testing circle number was probably due to the gradual loss of TiH_x in the thickness direction according to Equation (3) because of the formation of concentrated oxygen from OER, as a result, the general surface contact conductivity (which is a kind of average of the conductivities of TiH_x film and Ti oxide film) was decreased. Related mechanisms will be further discussed in Section 4 of this paper.

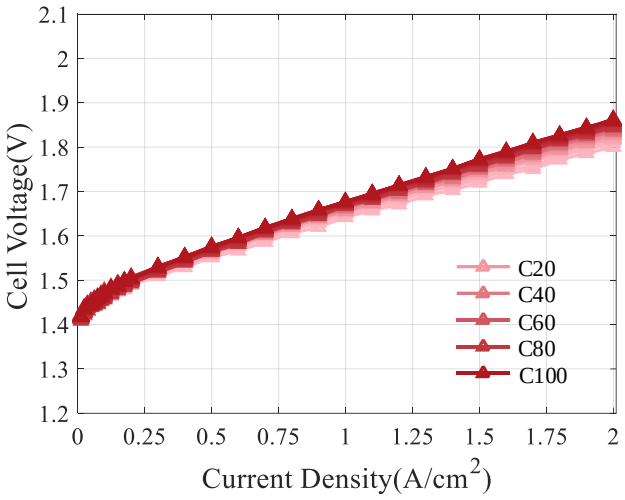

(a) I-V curve in 100 circles.

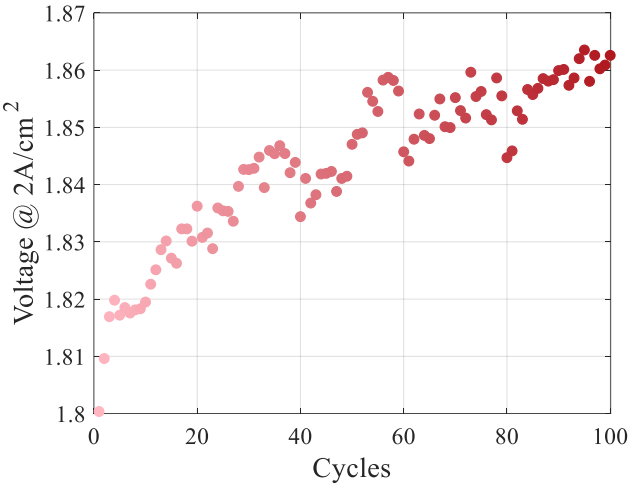

(b)Voltage changes @ 2A·cm^{-2} in 100 circles.

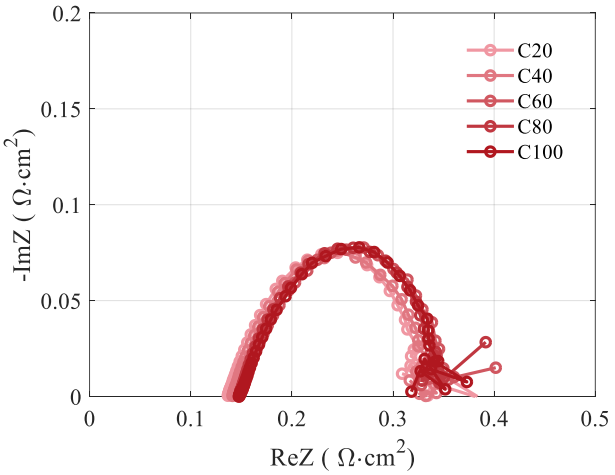

(c) EIS curve @ 0.1 A·cm^{-2} in 100 circles.

Fig. 5 Electrochemical performance of EA-48-15 PTL in 100 circles.

Moreover, Fig. 6 presents the XPS profiles without background (the raw data is referred to the Fig. S1 in the Supplemental Material) to explore the relative amount of certain valence of Ti between EA-48-15 PTL and 48-15 PTL. As shown in Fig. 6(a), both PTLs have similar intensity at the binding energy positions for Ti^{4+} and Ti^{0} before I-V testing. This means the surface composition of the certain valence of Ti is close to each other for these two newly fabricated PTLs. After both PTLs were assembled into their corresponding electrolyzers to test the corresponding I-V performances one time, both PTLs were dissembled from the electrolyzers, and XPS was conducted for the surface of each PTL (as shown in Fig. 6 (b)), which contacted with the anode catalyst layer; however, as shown in Fig. 6(b), after testing, the intensity of EA-48-15 PTL at the binding energy position for

Ti^{4+} drops dramatically as compared to that of the 48-15 PTL, which is considered due to the adhere of Nafion polymer of the anode catalyst layer onto the EA-48-15 PTL to weaken the X-ray signal to reach the actual surface of Ti fiber. Moreover, the distinct C-F bond signal at round 291eV [46] was detected on the surface of EA-48-15 PTL in the C1s XPS profile (without background) of Fig. 6(c), while no C-F bond signal was found on the surface of 48-15 PTL(i.e., no adhere of Nafion polymer), which is considered due to the poor contact between the 48-15 PTL surface and its corresponding anode catalyst layer. The raw data of Fig. 6(c) is referred to the Fig. S2 in the Supplemental Material. Based on the above information, more conclusions can be made: the 48-15 PTL leads to the worst I-V performance shown in Fig. 4, which means side reactions (accompanied by OER) might exist to be not only the reason for the poor contact between the 48-15 PTL and the anode catalyst layer but also for the reason of the biggest size of HF arc in the EIS curve. The mechanisms to relate the pretreatment process of 48-15 PTL to its poor electrolyzer performance based on the side reactions will be given in detail in Section 4.

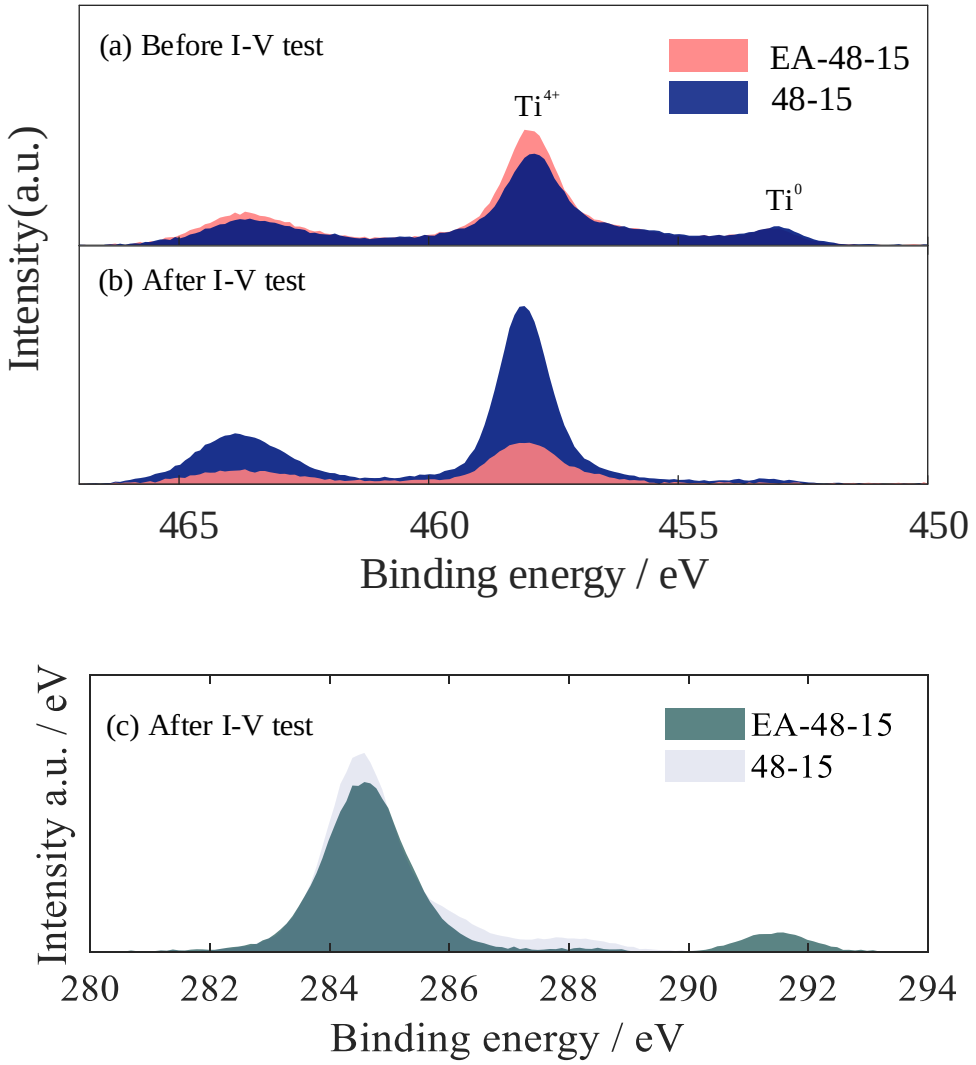

Fig. 6 XPS results of EA-48-15 and 48-15 PTL: (a) Ti 2p XPS results before I-V test (after ultrasound and acid etching). (b) after an I-V test. (c) C1s XPS results of carbon for EA-48-15 and 48-15 PTL after an I-V test.

3.3 Effect of electron conductive layer

Based on the analysis of Section 3.1 and Section 3.2, it can be concluded that a stable surface of Ti felt is important for the performance of the electrolyzer, which can avoid side reaction. To further prove this conclusion, 48-15-CP PTL and 48-15-Pt PTL were fabricated as shown in Table 2. As mentioned in Section 2.2, both the carbon paper of 48-15-CP PTL and the coated Pt on the 48-15-Pt contacted directly with the anode catalyst layers respectively during the I-V test.

As shown in Fig. 4(a), the electrolyzer with 48-15 PTL shows the poorest performance and the largest total EIS resistance and the HF arc. However, when integrating a Toray 060 carbon paper

with 48-15 PTL to form the two-layer 48-15-CP PTL or coating the 48-15 PTL with Pt to form the 48-15-Pt PTL, as shown in Fig. 7 (a), the performance of the corresponding electrolyzer is greatly improved, e.g., each performance can reach around 1.85V @2A·cm^{-2} (although, it is still 50 mV higher than that of EA-48-15). Furthermore, as comparing Fig. 7 (b) with Fig. 4 (b), only the OER kinetic resistance exists for these two PTLs with the conductive layer, i.e., the HF arc disappears after adding the conductive layer, i.e., the carbon paper and the Pt coating. This can be attributed to that the Ti corrosion reaction and other related side reactions in the electrolyzer with 48-15 PTL were eliminated after adding the electron conductive layer. However, the Pt layer was found not stable during the 15-circle testing: the HF arc appears again and the total resistance in the EIS curve also increases in Fig. S3 (b) in the Supplemental Material, which leads to the decreased performance for the electrolyzer as shown in Fig. S3 (a) in the Supplemental Material. However, as shown in Fig. S4 (b) in the Supplemental Material, after 15 circles of I-V testing, for the electrolyzer with 48-15-CP PTL, no HF arc appears, and the I-V performance changes less than that of 48-15-Pt as depicted in Fig. S4 (a). Therefore, there is a difference in protecting time-efficient between 48-15-Pt PTL and 48-15-CP PTL, and the related mechanisms will be discussed in Section 4.

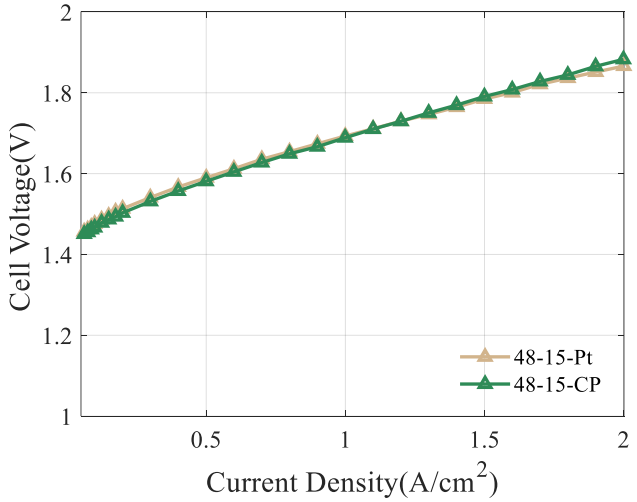

(a) I-V curves for the cases of 48-15-Pt PTL and 48-15-CP PTL.

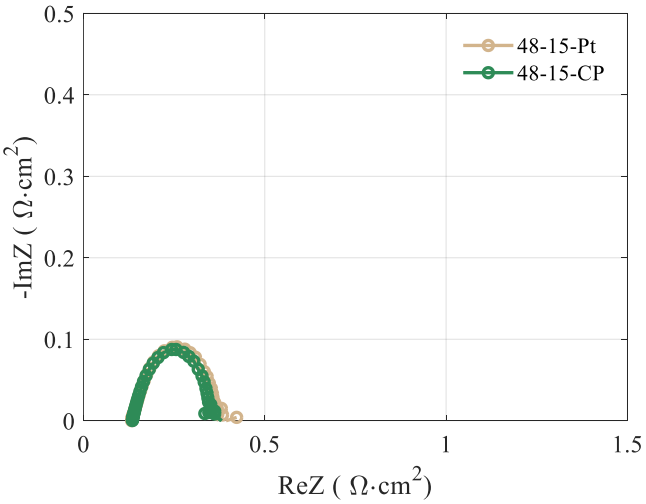

(b) EIS curve @ 0.1 A·cm^{-2} for the cases of 48-15-Pt PTL and 48-15-CP PTL.

Fig. 7 Electrochemical performance of the electrolyzers with 48-15-Pt PTL and 48-15-CP PTL in the first circle.

4 Discussion

The above results from electrochemical testing and physical characterization have found some phenomena that relate to the performance of the electrolyzer with different pretreatment processes of the Ti felt. In this Section, the mechanisms behind these phenomena are tried to be disclosed based on Fig. 8, in which different pretreatment processes for the pristine titanium felt (represented by the surface of a Ti fiber) are marked with a light red background, while the changes of PTL (i.e., the pretreated Ti felt, also represented by the surface of a Ti fiber) during the operation of an electrolyzer are distinguished by a blue background. When a mechanism is discussed, its corresponding sub-figure in Fig. 8 will be picked up to enlarge for seeing clearly.

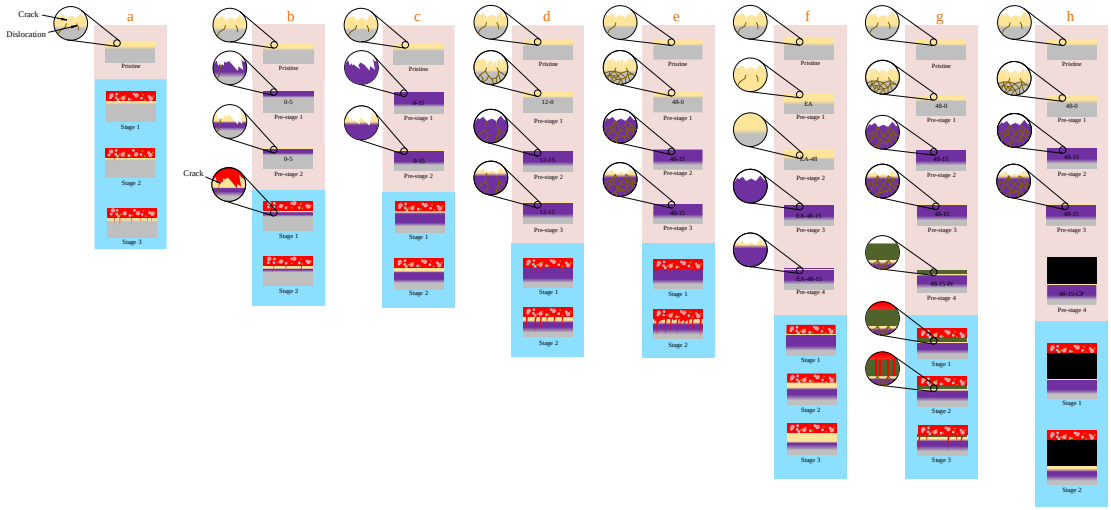

Fig. 8 Schematic diagram of the changes of titanium felts during different processes of pre-treatment and the changes of the resulting PTLs during the operations of electrolyzers. The colored patterns shown in Fig. 8 have the following meanings: represents Ti oxide film (mainly including the passivation layer, i.e., TiO_2); represents inner pure Ti metal; represents TiH_x; represents Pt; represents the fiber of carbon paper; represents anode catalyst layer; represents oxygen bubble; represents fluorion; represents hydrogen ion.

4.1 The mechanism of the state change of the Pristine PTL during the operation in an electrolyzer

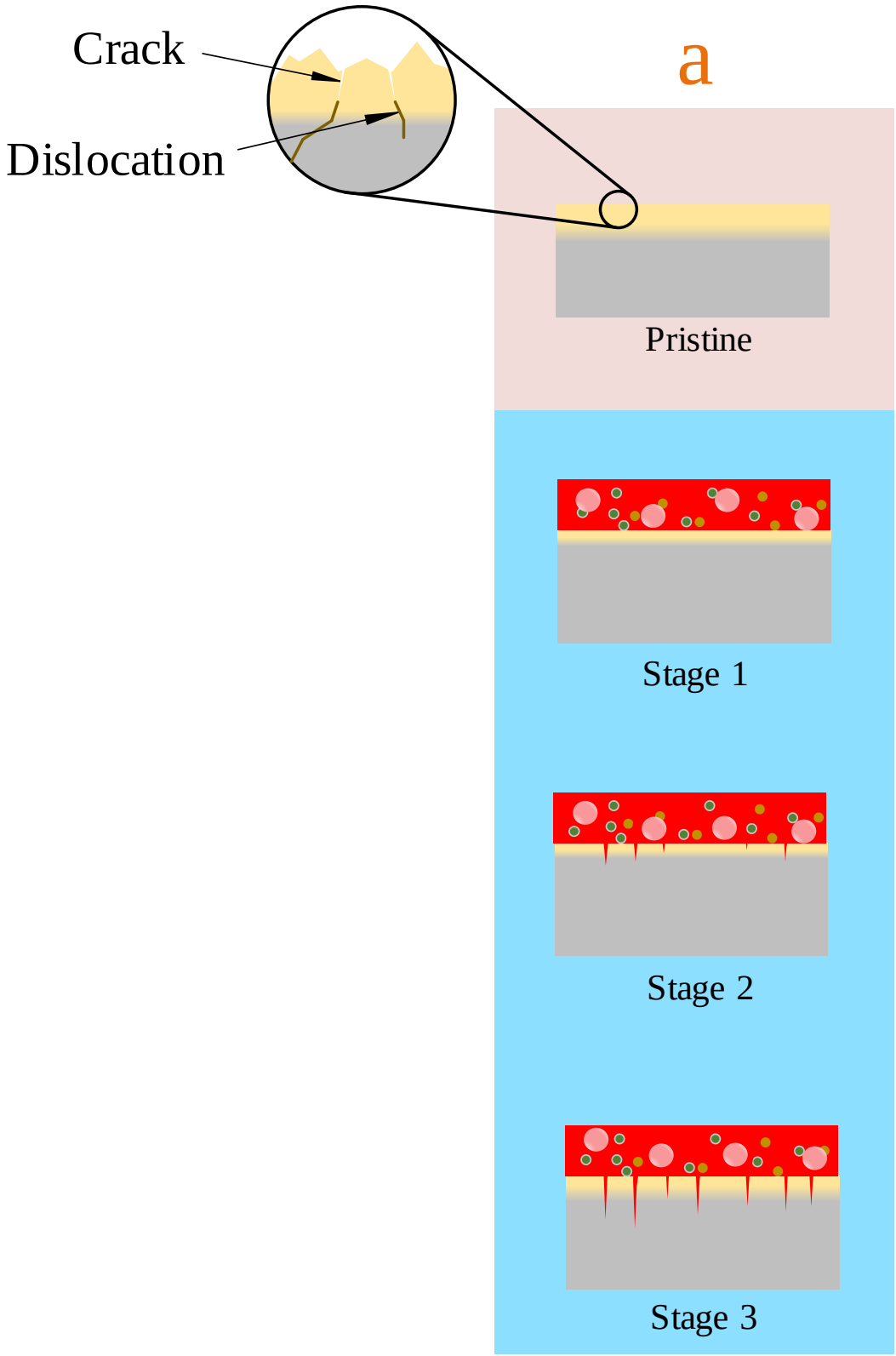

Fig. 8 (a) The possible internal structural state of the Pristine PTL (0-0 PTL) and its changes during the operation of the electrolyzer.

As found in Section 3.1, there is no significant difference in the HFR (ohmic resistance) for the electrolyzers using PTLs with and without acid etching, therefore, it is concluded that even the Ti oxide film (mainly including the passivation layer, i.e., TiO_2 due to its highest peak shown in Fig. 3) on the surface of the Pristine PTL (0-0 PTL) is very thin. As shown in Fig. S5(a), there are a lot of knuckles (pointed by the red arrows) on the fibers of the Pristine Ti felt, which might be aroused by the mechanical or thermal treatments during the production, therefore, these knuckles could induce dislocations (not visible through SEM observations) on the surface [47] of the Ti fibers, which could extend to form crack [48] in the very thin Ti oxide film (mainly including the passivation layer, i.e., TiO_2) on the surface of the Pristine felt, i.e., a desirable fully covered Ti oxide film cannot be formed due to mechanical manufacturing [49]. More importantly, dislocation and crack in the enlarged inset of Fig. 8 (a) are the places considered to enhance metal corroding [50], i.e., the enlarged inset presents the possible state for the fiber of the Pristine Ti felt after it is produced.

Moreover, after the Pristine PTL (0-0 PTL) is assembled in an electrolyzer which is then heated to its operating temperature and supplied with de-ionized water into its anode, it would experience further mechanical and thermal deformation due to the compression of the flow field plate, the expansion of MEA because of the elevated temperature, and the membrane swelling after absorbing the water. Therefore, some of the cracks shown in the inset of Fig. 8 (a) may extend and spread. At the very beginning of the electrolyzer operation (Stage 1 of Fig. 8 (a)), the cracks and the dislocations of the Ti oxide film (mainly including the passivation layer, i.e., TiO_2) are attacked easily [50] by the fluorion (released from the ionomer in the anode catalyst layer) based on the chemical reaction as shown in Equation (4) [51].

$$TiO_2 + 4H^+ + 6F^- \rightarrow TiF_6^{2-} + 2H_2O \quad (4)$$

As a result, the Ti oxide is dissolved, and the crack becomes larger. After that, the inner pure Ti metal is easily exposed (as depicted in the first cutting place of Stage 2 of Fig. 8 (a)), and it starts to undergo the electrochemical reaction based on Equation (5).

$$Ti \rightarrow Ti^{4+} + 4e^- \quad (5)$$

Hence, Ti^{4+} is released from the cutting place and the reaction is extended deeply into the Ti metal (i.e. the first cutting place of Stage 2 of Fig. 8 (a)) due to a lack of oxygen inside the cutting place for passivation, which is normally called crevice corrosion[52,53]. As a result, Equation (5) is considered as the corrosion reaction alongside OER in the anode, and it might be related to the

formation of the high frequency (HF) arc on the 0-0 curve of Fig. 1(b). This deduction is different from the current explanation for the HF arc, where it is normally explained as the charge transfer resistance of the electrons [34]. As the operation of the electrolyzer continues, on one hand, some formed cutting place goes deeper, and on the other hand, other cracks and dislocations are also attacked by the fluorion, resulting in more new cutting places extended into the Ti metal (as shown in Stage 3 of Fig. 8 (a)), where much more Ti^{4+} ions are released, therefore, the size of the HF arc on 0-0 curve of Fig. 1(b) is the biggest. Moreover, due to Equation (5), electrons are also released, which might hinder the OER reaction to some extent considering that the same total current is applied, therefore, the low-frequency arc (attributed to the rate-limiting step of OER [34]) on the 0-0 curve of Fig. 1 (b) appear larger compared to that of 0-15 curve in Fig. 1(b) (no HF arc appearing on 0-15 curve represents that no corrosion reaction of Equation (5) happens as mentioned above). In addition, during the process of operation, the released Ti^{4+} may diffuse to the top of the surface where O_2 is abundant, therefore, based on Equation (6) [53], TiO_2 may be generated again to make up for the dissolved TiO_2 layer (based on Equation (4)).

$$Ti^{4+} + O_2 + 4e^- \rightarrow TiO_2 \quad (6)$$

4.2 The mechanism of the effect of acid etching on the state change of PTL

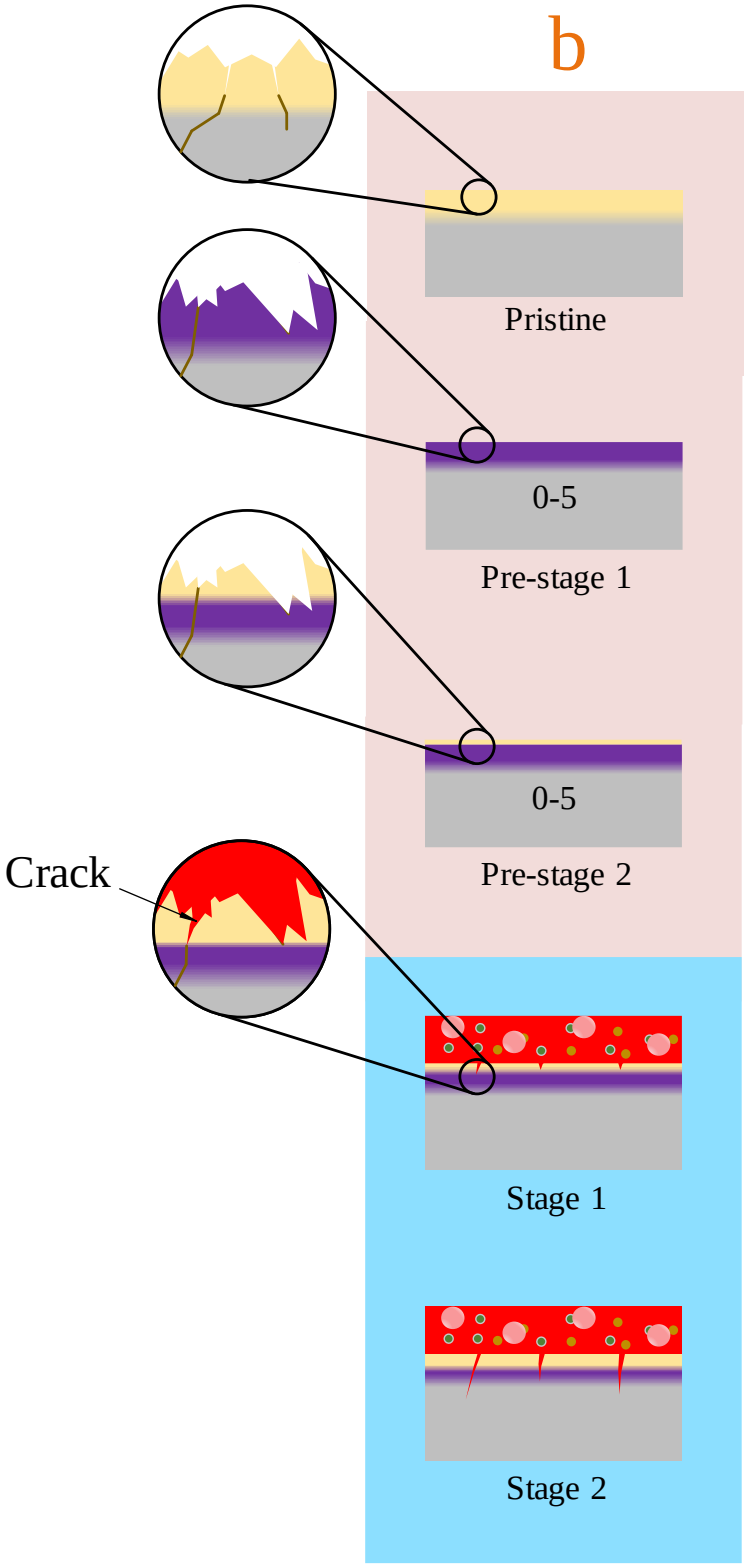

Fig. 8 (b) Pretreatment process of the 0-5 PTL and its changes during the operation of the electrolyzer.

As discussed in Section 3.1, during the etching period, the surface Ti oxide film (mainly including the passivation layer, i.e., TiO_2) is first removed by the concentrated hydrochloric acid solution, and then the inner Ti^0 (pure Ti metal) is exposed to react directly with hydrochloric acid to form TiH_x (Ti hydride) film according to Equation (1) and Equation (2) on the top surface of the Ti fiber. However, for the case of 0-5 PTL, the etching time is not long enough (only 5 minutes), which means that not all the dislocations in the pure Ti metal phase can be fully removed based on Equation (1), therefore, the residual dislocated Ti atoms absorb hydrogen atoms (Equation (2)) to keep some dislocations in the formed TiH_x film on the surface of the Ti fiber (as shown in the inset of the Pre-stage 1 of Fig. 8 (b)); As a result, the number of dislocations in the TiH_x film (the inset in Pre-stage 1 of Fig. 8 (b)) is less than that in the Ti oxide film of the Pristine Ti felt (the inset in Pristine of Fig. 8 (b)). Moreover, as mentioned in Section 3.1, once the acid etching pretreatment is finished, the 0-5 PTL is stored in the ambient air for further utilization, where part of the TiH_x film on the top surface of the Ti fiber can react with the oxygen in the air and is transformed again into the Ti oxide film (in which TiO_2 is the dominant part based on Fig. 3) according to Equation (3), as depicted in Pre-stage 2 of Fig. 8 (b). Therefore, part of the dislocation in the TiH_x film in Pre-stage 1 of Fig. 8 (b) is further transformed into the dislocation in the newly formed Ti oxide film (as shown in the inset of the Pre-stage 2 of Fig. 8(b)). The position where the dislocation exists in the Ti oxide film (as shown in the inset of the Pre-stage 2 of Fig. 8 (b)) probably has a higher chance of forming a crack after the 0-5 PTL is assembled in the electrolyzer to further experience the mechanical and thermal deformation during electrolysis, and the Ti oxides at the crack will also be attacked easily by the fluorion (released from the ionomer in the anode catalyst layer) based on the chemical reaction as shown in Equation (4). As a result, at the very beginning of the electrolyzer operation, TiO_2 near the dislocation is dissolved and a new crack appears (as shown in the inset of Stage 1 in Fig. 8 (b)). In the meantime, the underneath TiH_x can still react with the oxygen (derived from OER and diffusing through the upper Ti oxide film) according to Equation (3) to form a thicker Ti oxide film, i.e., the TiH_x film becomes thinner and thinner (as shown in Stage 2 of Fig. 8 (b) and compared to Stage 1 of Fig. 8 (b)). Furthermore, the continuous attack to the Ti oxide film from fluorion (Equation (4)) can accelerate the extension of the crack traversing the TiH_x layer (along the dislocation), directly into the inner pure Ti metal, i.e., cutting is formed in the inner pure Ti metal as shown in Stage 2 of Fig. 8 (b). After that, the inner pure Ti metal is easily exposed to release Ti^{4+}

based on the corrosion reaction shown in Equation (5). Therefore, the HF arc on the 0-5 curve of Fig. 1(b) still exists. However, due to the removal of part of the dislocations existing in the Pristine Ti felt and the formation of the protecting film of TiH_x during the 5-minute acid etching process, the chance of forming a cutting reaching the inner pure Ti metal becomes less, hence, less Ti^{4+} ions are released based on the corrosion reaction shown in Equation (4). As a result, the size of the HF arc for the case of 0-5 PTL is reduced when compared to that of 0-0 PTL (Pristine PTL) as shown in Fig. 1(b).

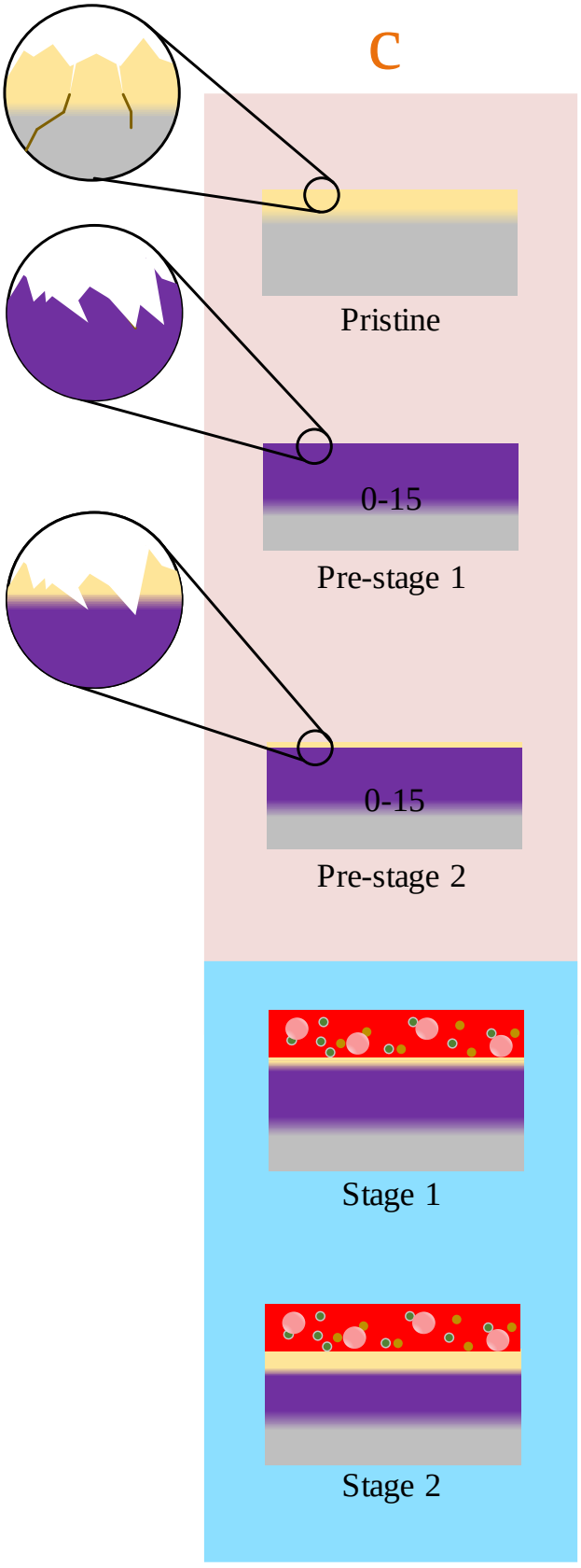

Fig. 8 (c) Pretreatment process of the 0-15 PTL and its changes during the operation of the electrolyzer.

When the etching time is increased to 15 minutes, after the removement of the Ti oxide film, more inner pure Ti metal layer is removed (Equation (1)), and a thicker TiH_x film is formed (Equation (2)) as shown in Pre-stage 1 of Fig. 8 (c), which is enough to restrict the residue of dislocations (due to the longer etching time) in the TiH_x film and the inner pure Ti metal after etching. And there is no dislocation on the top surface of the TiH_x film as shown in the inset of Pre-stage 1 of Fig. 8 (c), leading to no dislocations in the later formed new Ti oxide film (according to Equation (3)) as shown in the inset of Pre-stage 2. Therefore, there nearly exists no chance of having such a crack in the upper newly formed Ti oxide film, which can extend to the inner pure Ti metal along a dislocation by traversing the thick TiH_x layer.

After the 0-15 PTL is assembled in the electrolyzer, at the very beginning of the operation, due to the relatively thinner Ti oxide film as shown in Stage 1 of Fig. 8 (c), the underneath TiH_x can react relatively fast with the oxygen (derived from OER and diffusing through the upper Ti oxide film) according to Equation (3) to form a thicker Ti oxide film, i.e., the TiH_x film becomes thinner. However, not all the TiH_x can be transferred to Ti oxide in one I-V cycle, hence, there still exists a reasonable thickness of TiH_x film as shown in Stage 2 of Fig. 8 (c). As a result, the inner pure Ti metal is not exposed for the case of 0-15 PTL, hence no corrosion reaction of Equation (5) happens to release Ti^{4+}. Therefore, the HF arc for the case of 0-15 PTL disappears as shown in Fig. 1(b) to result in the best performance of 0-15 PTL as shown in Fig. 1(a).

4.3 The mechanism of the effect of ultrasonic cleaning on the state change of PTL

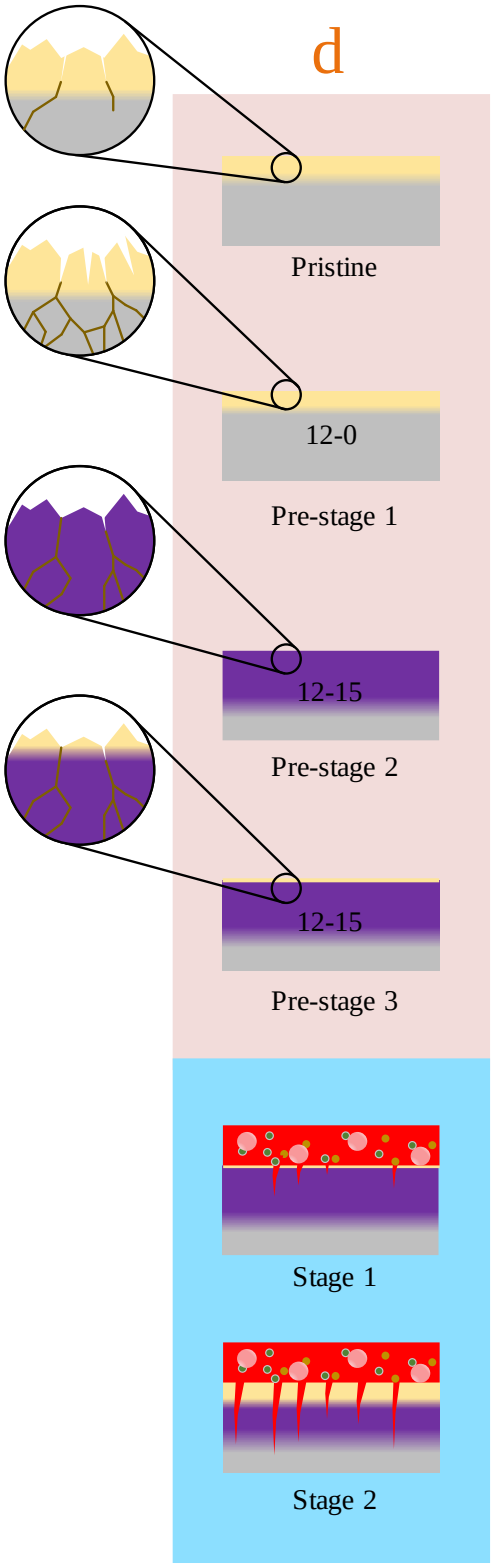

Fig. 8 (d) Pretreatment process of the 12-15 PTL and its changes during the operation of the electrolyzer.

When the ultrasonic cleaning is first introduced before acid etching, as shown in the inset of Pre-stage 1 of Fig. 8 (d), more cracks in the Ti oxide film on the surface of a fiber of the Pristine Ti felt and more serious dislocations in the inner pure Ti metal are induced due to the cavitation effect deriving from the ultrasonic energy [54,55]. Therefore, part of these serious dislocations (in the inner pure Ti metal) can be transformed into the dislocations crossing the formed TiH_x film as shown in the inset of Pre-stage 2 of Fig. 8 (d) during the reaction of Equation (2).

Later, after the PTL is exposed to the air, as shown in the inset of Pre-stage 3 of Fig. 8(d), some dislocations in the TiH_x film are further transformed into the dislocations in the newly formed Ti oxide thin film (according to Equation (3)). The positions where these dislocations exist in the upper Ti oxide film (as shown in the inset of the Pre-stage 3 of Fig. 8 (d)) have a higher chance of forming cracks after the 12-15 PTL is assembled in the electrolyzer to further experience the mechanical and thermal deformation during electrolysis, and the Ti oxides at the cracks and dislocations will also be attacked easily by the fluorion based on the chemical reaction as shown in Equation (4). As a result, at the very beginning of the electrolyzer operation, TiO_2 near the dislocations is dissolved and cracks appear and are induced into the inner part of the TiH_x film (as shown in Stage 1 of Fig. 8 (d)).

In the meantime, the underneath TiH_x can still react with the oxygen (derived from OER and diffusing through the upper Ti oxide film) according to Equation (3) to form a thicker Ti oxide film, i.e., the TiH_x film becomes thinner and thinner (as shown in Stage 2 of Fig. 8 (d) compared to Stage 1 of Fig. 8 (d)). Furthermore, the continuous attack to Ti oxide film from fluorions shown in Equation (4) can accelerate the extension and expansion of some cracks, traversing the TiH_x layer (along the dislocation), directly into the inner pure Ti metal, i.e., some cuttings are formed in the inner pure Ti metal as shown in Stage 2 of Fig. 8 (d).

After that, the inner pure Ti metal is easily exposed to release Ti^{4+} based on the corrosion reaction shown in Equation (5). Therefore, the HF arc on the 12-15 curve of Fig. 4 (b) appears again while as explained above no HF arc exists on the 0-15 curve of Fig 4 (b) or Fig.1 (b). However, due to the formation of a thicker protecting film of TiH_x during the 15-minute acid etching process, the chance of forming more cuttings reaching the inner pure Ti metal becomes less compared to 0-0 PTL, hence, less Ti^{4+} is released based on the corrosion reaction shown in Equation (5). As a result, the size of the HF arc for the case of 12-15 PTL is still smaller when compared to that of 0-0 PTL

(Pristine PTL) as shown in Fig. 1(b). Therefore, the performance of the electrolyzer with 12-15 PTL is poorer than that with 0-15 PTL but better than that with 0-0 PTL when comparing Fig. 1(a) with Fig. 4(a).

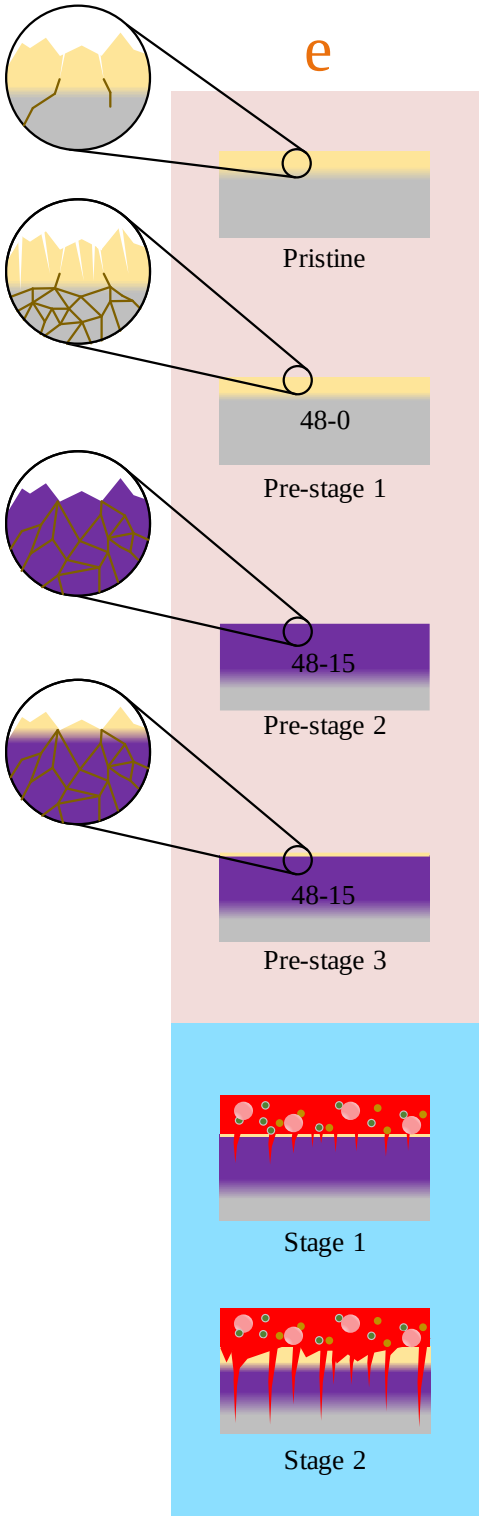

Fig. 8 (e) Pretreatment process of the 48-15 PTL and its changes during the operation of the electrolyzer.

As compared to the case of 12-15 PTL shown in Fig. 8 (d), it is easy to understand that, for the case of the 48-15 PTL as shown in Fig. 8 (e), the extremely long period of ultrasonic cleaning can cause much serious damage to the surface of a Ti PTL during the pretreatment process and the later operation in the electrolyzer. As a result, comparing Stage 2 of Fig. 8 (e) to Stage 2 of Fig. 8 (d), the formed Ti oxide film in the case of 48-15 PTL experiences a much stronger attack from the fluorions (released from the ionomer in the anode catalyst layer) based on the chemical reaction as shown in Equation (4), hence, the Ti oxide film becomes thinner and incomplete (as depicted in Stage 2 of Fig. 8 (e)), leading to serious destroy to the formed TiH_x film and more cuttings in the inner pure Ti metal. In consequence, much more Ti^{4+} is released (based on the corrosion reaction shown in Equation (5)) from more cuttings in the inner pure Ti metal as shown in Stage 2 of Fig. 8 (e). Therefore, the size of the HF arc for the case of 48-15 PTL becomes the largest as shown in Fig. 4 (b), resulting in the poorest performance as shown in Fig. 4 (a). Moreover, the processes to induce the serious damage in the PTL as depicted in Fig. 8 (e) is further supported by the SEM picture of 48-15 PTL as shown in Fig. S5 (b) in the Supplemental Material, in which a large number of turtle cracks (pointed by the red arrows) are distributed on the surface of the Ti fiber to prove that the surface has been seriously destroyed, leading to the poor contact between the 48-15 PTL and the anode catalyst layer as mentioned at the end of Section 3.2.

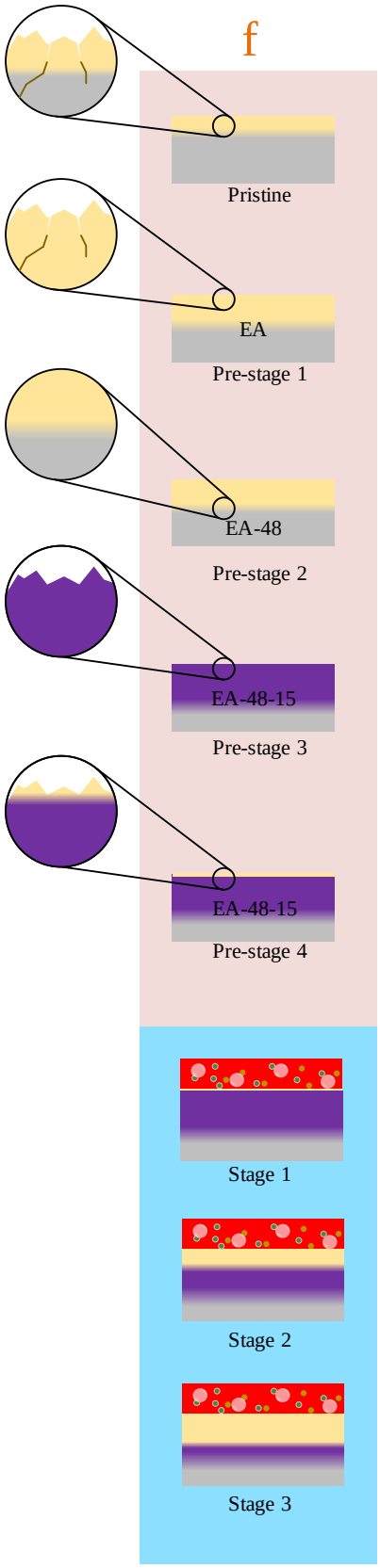

Fig. 8 (f) Pretreatment process of the EA-48-15 PTL and its changes during the operation of the electrolyzer.

When a pristine felt is exposed to the environment atmosphere (EA) for one week, the oxygen in the air has enough time to diffuse through the Ti oxide film on the surface of a Ti fiber to react with the inner pure Ti metal, therefore, as depicted in Pre-stage 1 of Fig. 8 (f), the Ti oxide film (mainly including the passivation layer, i.e., TiO_2, according to Fig. 3) becomes thick enough to supply enough protection for the inner pure Ti metal from the damage of cavitation even if the later ultrasonic cleaning time reaches 48 minutes due to the high strength of TiO_2 [43], i.e., the chance of forming new dislocations in the inner pure Ti metal during the 48-minute ultrasonic cleaning is pretty small as described by the inset of Pre-stage 2 of Fig. 8 (f). Moreover, the original dislocations existing in the inner pure Ti metal may be transformed into the dislocations in the thicker Ti oxide film during the one-week exposure as described in the inset of Pristine of Fig. 8 (f) and the inset of Pre-stage 1 of Fig. 8 (f). After conducting the 48-minute ultrasonic cleaning, it seems that the later 15-minute acid etching is long enough to first eliminate the much thicker Ti oxide film including the dislocations inside, and then to form a thick enough TiH_x film (Equation (2)) with the least dislocations, i.e., a good TiH_x film mentioned in Section 3.2 is formed as depicted in Pre-stage 3 of Fig. 8 (f). Later, after the pretreatment processes, the EA-48-15 PTL is stored in the atmosphere where part of the TiH_x film on the top surface of the Ti fiber can react with the oxygen and is transformed again into the Ti oxide film (according to Equation (3)) with the least dislocations inside as depicted in the inset of Pre-stage 4 of Fig. 8 (f).

Similar to Stage 1 and Stage 2 of Fig. 8 (c) for the case of 0-15 PLT, after the EA-48-15 PTL is assembled in the electrolyzer, at the very beginning of the operation, due to relatively thinner Ti oxide film (as shown in Stage 1 of Fig. 8 (f)), the underneath TiH_x can react relatively fast with the oxygen (derived from OER and diffusing through the upper Ti oxide film) according to Equation (3) to form a thicker Ti oxide film, i.e., the TiH_x film becomes thinner. However, when the Ti oxide film becomes thicker, it slows the oxygen diffusion to the deeper inside, i.e., the oxygen reaction rate with TiH_x film is reduced, hence, there still exists a reasonable thickness of TiH_x film as shown in Stage 2 of Fig. 8 (f). As a result, the inner pure Ti metal is not exposed for the case of EA-48-15 PTL, hence no side reaction of Equation (5) happens to release Ti^{4+}. Therefore, no HF arc for the case of EA-48-15 PTL appears at the first testing circle as shown in Fig. 4(b). Moreover, when the Ti oxide film grows thicker, it always contains few dislocations because the least dislocations are considered to exist in the good TiH_x film (as mentioned above). As a result, Ti oxide film has little

chance of being attacked by the fluorion, i.e., few cracks on the surface of the EA-48-15 PTL can be formed. This speculation is supported by two factors:

(1) The least cracks can be observed on the surface of Ti fibers as shown in the SEM picture of EA-48-15 PTL of Fig. S5(c) in the Supplemental Material, matching well the processes depicted in Fig.8(f) and indicating the integrity of the surface structure of EA-48-15 PTL after testing. This may lead to good contact between the fibers of the EA-48-15 PTL and the anode catalyst layer. As a result, the ohmic resistance for the case of EA-48-15 PTL is the smallest as shown in Fig. 4(b) and 4(c). Moreover, when integrating the disappearance of HF arc with the smallest ohmic resistance (HFR) as shown in Fig. 4(b) and 4(c), the electrolyzer with EA-48-15 PTL no doubt shows the best performance as depicted in Fig. 4(a).

(2) The SEM and EDS characterization were conducted for both EA-48-15 PTL and 48-15 PTL after the first I-V testing circles were finished for the electrolyzers with corresponding PTLs. Based on the EDS analysis shown in Fig. S6(c) in the Supplemental Material, it can be concluded that the Ti oxide film on the EA-48-15 PTL is thicker than that on the 48-15 PTL because the region of the relative content changes of Ti and O elements is wider for the EA-48-15 PTL (around 1700 nm) as compared to that for the 48-15 PTL (around 700 nm). This also explains that the least attack is exerted on the Ti oxide film from the fluorion due to the least dislocations existing in the EA-48-15 PTL. Therefore, a thicker Ti oxide film existed on EA-48-15 PTL; on the contrary, for the case of 48-15 PTL, the number of dislocations is much larger, as depicted in Pre-stage 3 of Fig. 8 (e). Therefore, the Ti oxide film on the upper surface of a Ti fiber is seriously attacked by fluorion according to Equation (4), as a result, the Ti oxide film becomes thinner and incomplete as depicted in Stage 2 of Fig. 8 (e).

Moreover, during the total of 100 I-V testing circles for the electrolyzer with EA-48-15 PTL as shown in Fig. 5(a), i.e., a long testing time, the oxygen (derived from OER) can still diffuse (although slower and slower) through the Ti oxide film to react with the underneath TiH_x according to Equation (3) to further thickening the Ti oxide film; moreover, as mentioned above, the good TiH_x film formed on EA-48-15 PTL contains the least dislocations, resulting in few dislocations in the formed Ti oxide film. As a result, during the 100 I-V testing circles, it is considered that only

the Ti oxide film is getting thicker and thicker, and TiH_x film is still complete but getting thinner and thinner as depicted in Stage 3 of Fig. 8 (f), i.e., no other side reactions happen to form cracks or cuttings in the PTL. Therefore, the ohmic resistance is increased due to the thicker Ti oxide film (mainly including the passivation layer, i.e., TiO_2, according to Fig. 3). This is the reason for the increased ohmic resistance as shown in Fig 5 (c), the deceased performance as shown in Fig. 5(a) and Fig. 5(b), and no change in the size of kinetic resistance arc as shown in Fig 5(c).

4.4 The mechanism of the effect of the electron conductive layer on the state change of PTL

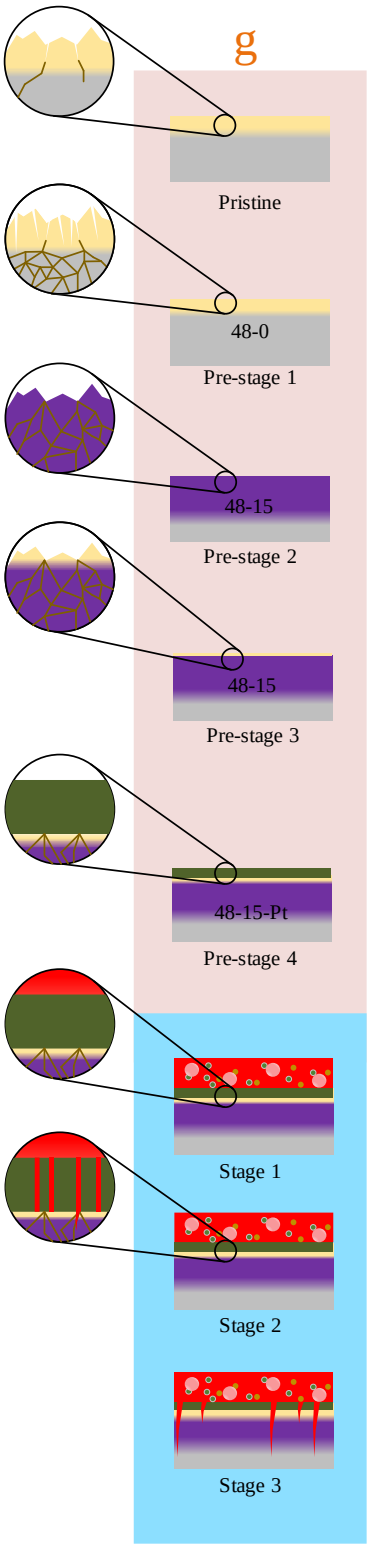

Fig. 8 (g) Pretreatment process of the 48-15-Pt PTL and its changes during the operation of the electrolyzer.

A new 48-15 PTL is further fabricated, therefore, the states of the PTL before Pre-stage 3 as shown in Fig. 8 (g) are the same as those shown in Fig. 8 (e). Later, a 10 nm thickness Pt film is deposited on the 48-15 PTL as shown in Pre-stage 4 of Fig. 8 (g) to form the 48-15-Pt PTL. Therefore, at the very beginning of the electrolyzer operation (Stage 1 of Fig. 8 (g)), due to the protection of the Pt film, the side reactions such as Equation (4) and Equation (5) (Ti corrosion reaction) do not happen. As a result, compared to the performance of the electrolyzer with 48-15 PTL shown in Fig. 4, as shown in Section 3.2, the HF arc disappears and the kinetics resistance arc becomes smaller (Fig. 7(b)), resulting in improved I-V performance for the electrolyzer with 48-15-Pt PTL (Fig. 7(a)). However, there are a lot of dislocations in the Ti oxide film and TiH_x film as shown in the inset of Pre-stage 3 of Fig. 8 (g); hence, when 15-circle testing is further conducted, these dislocations may induce the cracks (as shown in the inset of Stage 2 of Fig. 8 (g)) in the Pt film, especially considering that both the mechanical and thermal deformation also exerts on the PTL during the electrolyzer operation. In consequence, the anode catalyst layer can contact with the Ti oxide film directly through these Pt cracks (as shown in the inset of Stage 2 of Fig. 8 (g)). Therefore, fluorion (released from the ionomer in the anode catalyst layer) starts to attack the upper Ti oxide film based on the chemical reaction as shown in Equation (4), and finally cracks are formed in the Ti oxide film and TiH_x film to induce the formation of cuttings in the inner pure Ti metal (as shown in Stage 3 of Fig. 8 (g), and also referring to Fig. 8 (d) and 8(e) and related context). Therefore, the inner pure Ti metal is exposed to release Ti^{4+} based on the corrosion reaction shown in Equation (5), resulting in the re-appearance of HF arc (Fig. S3 (b)) in the Supplemental Material) and the reduced I-V performance (Fig. S3 (a) in the Supplemental Material) after the 15-circle testing.

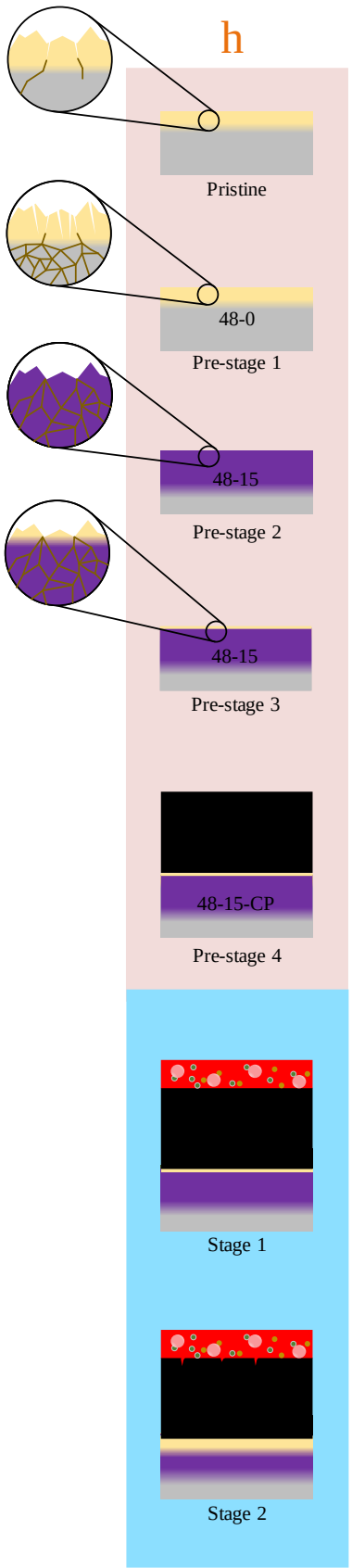

Fig. 8 (h) Pretreatment process of the 48-15-CP PTL and its changes during the operation of the electrolyzer.

Another new 48-15 PTL is further fabricated, therefore, the states of the PTL before pre-stage 3 as shown in Fig. 8 (h) are the same as those shown in Fig. 8 (e). Toray 060 carbon paper (0.19 mm in thickness) is covered on the 48-15 PTL as shown in pre-stage 4 of Fig. 8 (h) to form the 48-15-CP PTL. The 0.19 mm thickness of the carbon paper is pretty large when considering that the Pt coating film is only 10 nm on the 48-15-Pt PTL. Moreover, the concentration of fluorion is diluted by the de-ionized water in the anode to a low level (due to water existing in the carbon paper); therefore, the fluorion (released from the ionomer in the anode catalyst layer) is difficult to reach the Ti oxide film (as shown in stage 1 of Fig. 8 (h)). As a result, the upper Ti oxide film is hardly attacked by fluorion [56], i.e., the reaction shown in Equation (4) may not happen. Hence, cracks are hardly formed in the Ti oxide film and TiH_x film, and no cuttings in the inner pure Ti metal are induced. In consequence, the corrosion reaction of Ti (Equation (5)) does not happen. Thus, compared to the performance of the electrolyzer with 48-15 PTL shown in Fig. 4, the HF arc always disappears. Moreover, the high anode potential can induce the corrosion of the carbon paper, i.e., cracks may appear on the fiber of the carbon paper (as depicted in Stage 2 of Fig. 8 (h)), leading to poorer contact between the carbon paper and the anode catalyst layer. And in the meantime, the TiH_x can react with the oxygen (derived from OER and diffusing through the carbon paper and the upper Ti oxide film) according to Equation (3) to form a thicker Ti oxide film, i.e., the TiH_x film becomes thinner, leading to the increased ohmic resistance; the above two reasons may explain the slightly increased ohmic resistance (Fig. S4(b) in the Supplemental Material) and deceased I-V performance (Fig. S4(a)) after the 15-circle testing of the electrolyzer with 48-15-CP PTL.

5 Conclusion

In this research, ten anode PTLs were fabricated based on different designs of pretreatment processes including acid etching and ultrasonic cleaning. By integrating the electrochemical testing for single electrolyzers using these ten different PTLs with the physical characterizations for the PTLs, the effects of the pretreatment processes on the performance of PEMWEs were studied, and related mechanisms were disclosed. Some major conclusions are as follows:

(1) The purpose of acid etching was to eliminate the Ti oxide film on the top surface of a

pristine Ti felt, in which dislocations and cracks might exist due to manufacturing, and to form a good TiH_x film for protection.

(2) It was the dislocations and cracks that were found to induce side reactions such as the dissolution of Ti oxide film and the Ti corrosion inside the pure Ti metal during the operation of an electrolyzer, which resulted in the appearance of the high frequency (HF) arc in the EIS curve and worsened the performance of the electrolyzer.

(3) Ultrasonic cleaning was found to lead to the formation of more dislocations or cracks, i.e., worsening the surface condition of Ti felt during the pretreatment process and the later performance in the electrolyzers.

(4) Exposing a pristine Ti felt into the environment atmosphere for a long time was considered to be a good method to form a thicker Ti oxide film on the surface of Ti felt, leading to the protection of inner pure Ti metal from forming more dislocations when the ultrasonic energy shock was exerted. More importantly, during the long-time exposure, the dislocations (from manufacturing) in the inner pure metal were considered to be converted to those in the Ti oxide film on the surface of the Ti felt, thus, they could be eliminated or diminished during the later acid etching process to supply the good surface condition to form a good TiH_x film.

(5) Coating (electron conductive layer) exerted on a PTL with poor surface condition (i.e., existing a lot of dislocations or cracks) might only supply temporary protection unless the coating was extremely thick. Therefore, good surface condition of Ti felt should be first acquired based on suitable pretreatment processes before the coating was applied.

Acknowledgment

This research was supported by Shanghai Natural Science Foundation (No. 16ZR1417000) and the program of the top project unveiled by Inner Mongolia Autonomous Region (No. 22JBGS0027).

References

[1] Hermesmann M, Müller TE. Green, Turquoise, Blue, or Grey? Environmentally friendly Hydrogen Production in Transforming Energy Systems. Progress in Energy and Combustion Science 2022;90:100996. https://doi.org/10.1016/j.pecs.2022.100996.

[2] García-Valverde R, Espinosa N, Urbina A. Optimized method for photovoltaic-water electrolyser direct coupling. International Journal of Hydrogen Energy 2011;36:10574–86. https://doi.org/10.1016/j.ijhydene.2011.05.179.

[3] Laoun B, Khellaf A, Naceur MW, Kannan AM. Modeling of solar photovoltaic-polymer electrolyte membrane electrolyzer direct coupling for hydrogen generation. International Journal of Hydrogen Energy 2016;41:10120–35. https://doi.org/10.1016/j.ijhydene.2016.05.041.

[4] Ramadan M. A review on coupling Green sources to Green storage (G2G): Case study on solar-hydrogen coupling. International Journal of Hydrogen Energy 2021;46:30547–58. https://doi.org/10.1016/j.ijhydene.2020.12.165.

[5] Carmo M, Fritz DL, Mergel J, Stolten D. A comprehensive review on PEM water electrolysis. International Journal of Hydrogen Energy 2013;38:4901–34. https://doi.org/10.1016/j.ijhydene.2013.01.151.

[6] Teuku H, Alshami I, Goh J, Masdar MS, Loh KS. Review on bipolar plates for low-temperature polymer electrolyte membrane water electrolyzer. International Journal of Energy Research 2021;45:20583–600. https://doi.org/10.1002/er.7182.

[7] Li H, Fujigaya T, Nakajima H, Inada A, Ito K. Optimum structural properties for an anode current collector used in a polymer electrolyte membrane water electrolyzer operated at the boiling point of water. Journal of Power Sources 2016;332:16–23. https://doi.org/10.1016/j.jpowsour.2016.09.086.

[8] Steen SM, Mo J, Kang Z, Yang G, Zhang F-Y. Investigation of titanium liquid/gas diffusion layers in proton exchange membrane electrolyzer cells. International Journal of Green Energy 2017;14:162–70. https://doi.org/10.1080/15435075.2016.1253582.

[9] Stiber S, Balzer H, Wierhake A, Wirkert FJ, Roth J, Rost U, et al. Porous Transport Layers for Proton Exchange Membrane Electrolysis Under Extreme Conditions of Current Density, Temperature, and Pressure. Advanced Energy Materials 2021;11:2100630. https://doi.org/10.1002/aenm.202100630.

[10] Bernt M, Gasteiger HA. Influence of Ionomer Content in IrO_2 /TiO_2 Electrodes on PEM Water Electrolyzer Performance. J Electrochem Soc 2016;163:F3179–89. https://doi.org/10.1149/2.0231611jes.

[11] Schuler T, Ciccone JM, Krentscher B, Marone F, Peter C, Schmidt TJ, et al. Hierarchically Structured Porous Transport Layers for Polymer Electrolyte Water Electrolysis. Advanced Energy Materials 2020;10:1903216. https://doi.org/10.1002/aenm.201903216.

[12] Mo J, Steen S, Han B, Kang Z, Terekhov A, Zhang F-Y, et al. Investigation of titanium felt transport parameters for energy storage and hydrogen/oxygen production. 13th International Energy Conversion Engineering Conference, Orlando, FL: American Institute of Aeronautics and Astronautics; 2015. https://doi.org/10.2514/6.2015-3914.

[13] Peng X, Satjaritanun P, Taie Z, Wiles L, Keane A, Capuano C, et al. Insights into Interfacial and Bulk Transport Phenomena Affecting Proton Exchange Membrane Water Electrolyzer Performance at Ultra-Low Iridium Loadings. Advanced Science 2021;8:2102950. https://doi.org/10.1002/advs.202102950.

[14] Mo J, Steen SM, Retterer S, Cullen DA, Terekhov A, Zhang F-Y. Mask-Patterned Wet Etching of Thin Titanium Liquid/Gas Diffusion Layers for a PEMEC. ECS Trans 2015;66:3–10. https://doi.org/10.1149/06624.0003ecst.

[15] Kang Z, Mo J, Yang G, Retterer ST, Cullen DA, Toops TJ, et al. Investigation of thin/well-tunable liquid/gas diffusion layers exhibiting superior multifunctional performance in low-temperature electrolytic water splitting. Energy Environ Sci 2017;10:166–75. https://doi.org/10.1039/C6EE02368A.

[16] Liu C, Carmo M, Bender G, Everwand A, Lickert T, Young JL, et al. Performance enhancement of PEM electrolyzers through iridium-coated titanium porous transport layers. Electrochemistry Communications 2018;97:96–9. https://doi.org/10.1016/j.elecom.2018.10.021.

[17] Weber CC, Schuler T, De Bruycker R, Gubler L, Büchi FN, De Angelis S. On the role of porous transport layer thickness in polymer electrolyte water electrolysis. Journal of Power Sources Advances 2022;15:100095. https://doi.org/10.1016/j.powera.2022.100095.

[18] Schuler T, Schmidt TJ, Büchi FN. Polymer Electrolyte Water Electrolysis: Correlating Performance and Porous Transport Layer Structure: Part II. Electrochemical Performance Analysis. J Electrochem Soc 2019;166:F555–65. https://doi.org/10.1149/2.1241908jes.

[19] Li Y, Feng B, Li G, Qi J, Zhao D, Mu Y. Optimal distributed generation planning in active distribution networks considering integration of energy storage. Applied Energy 2018;210:1073–81. https://doi.org/10.1016/j.apenergy.2017.08.008.

[20] Liu C, Shviro M, Gago AS, Zaccarine SF, Bender G, Gazdzicki P, et al. Exploring the Interface of Skin-Layered Titanium Fibers for Electrochemical Water Splitting. Adv Energy Mater 2021:10.

[21] Wang W, Li K, Ding L, Yu S, Xie Z, Cullen DA, et al. Exploring the Impacts of Conditioning on Proton Exchange Membrane Electrolyzers by *In Situ* Visualization and Electrochemistry Characterization. ACS Appl Mater Interfaces 2022;14:9002–12. https://doi.org/10.1021/acsami.1c21849.

[22] Park YJ, Lee J, Park YS, Yang J, Jang MJ, Jeong J, et al. Electrodeposition of High-Surface-Area IrO2 Films on Ti Felt as an Efficient Catalyst for the Oxygen Evolution Reaction. Front Chem 2020;8:593272. https://doi.org/10.3389/fchem.2020.593272.

[23] Bystron T, Vesely M, Paidar M, Papakonstantinou G, Sundmacher K, Bensmann B, et al. Enhancing PEM water electrolysis efficiency by reducing the extent of Ti gas diffusion layer passivation. J Appl Electrochem 2018;48:713–23. https://doi.org/10.1007/s10800-018-1174-6.

[24] Gao H, Yu M, Chen X, Xiao G, Chen C, Liu B, et al. Ultrasonic Induced Refinement of Induction Heated Oxide Coating on Titanium. Coatings 2021;11:812.

https://doi.org/10.3390/coatings11070812.

[25] Xu H, Zhang Q, Zheng C, Yan W, Chu W. Application of ultrasonic wave to clean the surface of the TiO2 nanotubes prepared by the electrochemical anodization. Applied Surface Science 2011;257:8478–80. https://doi.org/10.1016/j.apsusc.2011.04.135.

[26] Yousif QA, Haran NH. Ultrasound effects on titanium dioxide compact layer and its application of dye-sensitized solar cell. Optik 2022;270:169964. https://doi.org/10.1016/j.ijleo.2022.169964.

[27] Song SL, Li DG, Chen DR, Liang P. The role of Ti in cavitation erosion and corrosion behaviours of NAB alloy in 3.5 % NaCl solution. Journal of Alloys and Compounds 2022;919:165728. https://doi.org/10.1016/j.jallcom.2022.165728.

[28] Seo D-I, Lee J-B. Effects of competitive anion adsorption (Br− or Cl−) and semiconducting properties of the passive films on the corrosion behavior of the additively manufactured Ti–6Al–4V alloys. Corrosion Science 2020;173:108789. https://doi.org/10.1016/j.corsci.2020.108789.

[29] Turner W. Electroplating of titanium and titanium alloy. DE3161909D1, 1984.

[30] Tu Z, LI N, Zhu Y. Application and technology on surface treatment of titanium and titanium alloys 2010.

[31] Pham CV, Escalera-López D, Mayrhofer K, Cherevko S, Thiele S. Essentials of High Performance Water Electrolyzers – From Catalyst Layer Materials to Electrode Engineering. Adv Energy Mater 2021;11:2101998. https://doi.org/10.1002/aenm.202101998.

[32] Bautkinova T, Utsch N, Bystron T, Lhotka M, Kohoutkova M, Shviro M, et al. Introducing titanium hydride on porous transport layer for more energy efficient water electrolysis with proton exchange membrane. Journal of Power Sources 2023;565:232913. https://doi.org/10.1016/j.jpowsour.2023.232913.

[33] Doan TL, Lee HE, Kim M, Cho WC, Cho HS, Kim T. Influence of IrO2/TiO2 coated titanium porous transport layer on the performance of PEM water electrolysis. Journal of Power Sources 2022;533:231370. https://doi.org/10.1016/j.jpowsour.2022.231370.

[34] Stiber S, Sata N, Morawietz T, A. Ansar S, Jahnke T, K. Lee J, et al. A high-performance, durable and low-cost proton exchange membrane electrolyser with stainless steel components. Energy & Environmental Science 2022;15:109–22. https://doi.org/10.1039/D1EE02112E.

[35] Kang Z, Schuler T, Chen Y, Wang M, Zhang F-Y, Bender G. Effects of interfacial contact under different operating conditions in proton exchange membrane water electrolysis. Electrochimica Acta 2022;429:140942. https://doi.org/10.1016/j.electacta.2022.140942.

[36] Hu M, Sui S, Zhu X, Yu Q, Cao G, Hong X, et al. A 10kW class PEM fuel cell stack based on the catalyst-coated membrane (CCM) method. International Journal of Hydrogen Energy 2006;31:1010–8. https://doi.org/10.1016/j.ijhydene.2006.02.018.

[37] Ren N, Wang G, Liu H, Ohachi T. In situ synthesis of TiH2 layer on metallic titanium foil through gaseous hydrogen free acid-hydrothermal method. Materials Research Bulletin 2014;50:379–84. https://doi.org/10.1016/j.materresbull.2013.11.002.

[38] Gromov AR, Kouznetsova NN, Yudina SL, Lunin VV. The investigation of titanium hydride oxidation process. Journal of Alloys and Compounds 1997;261:269–72. https://doi.org/10.1016/S0925-8388(97)00193-X.

[39] Samal S, Cho S, Park DW, Kim H. Thermal characterization of titanium hydride in thermal oxidation process. Thermochimica Acta 2012;542:46–51.

https://doi.org/10.1016/j.tca.2012.02.010.

[40] Rittmeyer P, Wietelmann U. Hydrides. Ullmann's Encyclopedia of Industrial Chemistry, John Wiley & Sons, Ltd; 2000. https://doi.org/10.1002/14356007.a13_199.

[41] Miguel Martín-Martínez J. Rubber base adhesives. Adhesion Science and Engineering, Elsevier; 2002, p. 573–675. https://doi.org/10.1016/B978-044451140-9/50013-5.

[42] Kelkar SM. Using X-ray Imaging Techniques to Determine Density of Foods n.d.

[43] Li DG, Wang JD, Chen DR, Liang P. The role of passive potential in ultrasonic cavitation erosion of titanium in 1M HCl solution. Ultrasonics Sonochemistry 2016;29:279–87. https://doi.org/10.1016/j.ultsonch.2015.09.018.

[44] Lettenmeier P, Kolb S, Sata N, Fallisch A, Zielke L, Thiele S, et al. Comprehensive investigation of novel pore-graded gas diffusion layers for high-performance and cost-effective proton exchange membrane electrolyzers. Energy Environ Sci 2017;10:2521–33. https://doi.org/10.1039/C7EE01240C.

[45] Ito M, Setoyama D, Matsunaga J, Muta H, Kurosaki K, Uno M, et al. Electrical and thermal properties of titanium hydrides. Journal of Alloys and Compounds 2006;420:25–8. https://doi.org/10.1016/j.jallcom.2005.10.032.

[46] Palchan I, Crespin M, Estrade-Szwarckopf H, Rousseau B. Graphite fluorides: An XPS study of a new type of C-F bonding. Chemical Physics Letters 1989;157:321–7. https://doi.org/10.1016/0009-2614(89)87255-0.

[47] Zhang Y, Yu T, Xu R, Thorborg J, Liu W, Tischler J, et al. Local residual stresses and microstructure within recrystallizing grains in iron. Materials Characterization 2022;191:112113. https://doi.org/10.1016/j.matchar.2022.112113.

[48] Noyan IC, Cohen JB. The Nature of Residual Stress and its Measurement. In: Kula E, Weiss V, editors. Residual Stress and Stress Relaxation, Boston, MA: Springer US; 1982, p. 1–17. https://doi.org/10.1007/978-1-4899-1884-0_1.

[49] Li L, Qiao Y, Zhang L, Li C, Liu Z, Ma R, et al. Effects of cavitation erosion-induced surface damage on the corrosion behaviour of TA31 Ti alloy. Ultrasonics Sonochemistry 2023;98:106498. https://doi.org/10.1016/j.ultsonch.2023.106498.

[50] Macdonald DD. 6 - The electrochemical nature of stress corrosion cracking. In: Féron D, Staehle RW, editors. Stress Corrosion Cracking of Nickel Based Alloys in Water-cooled Nuclear Reactors, Woodhead Publishing; 2016, p. 239–94. https://doi.org/10.1016/B978-0-08-100049-6.00006-9.

[51] Li Y, Xu J. Is niobium more corrosion-resistant than commercially pure titanium in fluoride-containing artificial saliva? Electrochimica Acta 2017;233:151–66. https://doi.org/10.1016/j.electacta.2017.03.015.

[52] Xu W, Zhang B, Addison O, Wang X, Hou B, Yu F. Mechanically-assisted crevice corrosion and its effect on materials degradation. Corrosion Communications 2023. https://doi.org/10.1016/j.corcom.2023.01.002.

[53] Standish TE, Yari M, Shoesmith DW, Noël JJ. Crevice Corrosion of Grade-2 Titanium in Saline Solutions at Different Temperatures and Oxygen Concentrations. J Electrochem Soc 2017;164:C788. https://doi.org/10.1149/2.0941713jes.

[54] Ju DY, Han B. Investigation of water cavitation peening-induced microstructures in the near-surface layer of pure titanium. Journal of Materials Processing Technology 2009;209:4789–94. https://doi.org/10.1016/j.jmatprotec.2008.12.006.

[55] Fernández-Domene RM, Blasco-Tamarit E, García-García DM, García-Antón J. Cavitation corrosion and repassivation kinetics of titanium in a heavy brine LiBr solution evaluated by using electrochemical techniques and Confocal Laser Scanning Microscopy. Electrochimica Acta 2011;58:264–75. https://doi.org/10.1016/j.electacta.2011.09.034.

[56] Is niobium more corrosion-resistant than commercially pure titanium in fluoride-containing artificial saliva? Electrochimica Acta 2017;233:151–66. https://doi.org/10.1016/j.electacta.2017.03.015.

CRediT author statement

Zheng Zhou: Conceptualization, Test, Methodology, Validation, Investigation, Writing - Original Draft

Kequan Ye: Test, Validation, Investigation, Formal analysis

Qing Wang: Test, Validation, Investigation

Mingruo Hu: Conceptualization, Methodology, Validation, Writing, Formal analysis, Investigation, Funding acquisition, Project administration

Xiaoyu Hu: Test, Validation

Sibo Wang: Test, Validation, Investigation

Chengyu Hu: Test, Validation

Guangyi Cao: Conceptualization, Methodology

Declaration of interests

☒The authors declare that they have no known competing financial interests or personal relationships that could have appeared to influence the work reported in this paper.

☐The authors declare the following financial interests/personal relationships which may be considered as potential competing interests: